

# Scalable Single-Cell Gene Expression Generation with Latent Diffusion Models

Giovanni Palla<sup>‡a</sup> , Sudarshan Babu<sup>b</sup> , Payam Dibaeinia<sup>b</sup> , James D. Pearce<sup>a</sup> ,  
Donghui Li<sup>a</sup> , Aly A. Khan<sup>b</sup> , Theofanis Karaletsos<sup>‡\*a</sup> ,  
and Jakub M. Tomczak<sup>‡\*a</sup> 

<sup>a</sup> Chan Zuckerberg Initiative, Redwood City, CA

<sup>b</sup> Chan Zuckerberg Biohub, Chicago, IL

## Abstract

Computational modeling of single-cell gene expression is crucial for understanding cellular processes, but generating realistic expression profiles remains a major challenge. This difficulty arises from the count nature of gene expression data and complex latent dependencies among genes. Existing generative models often impose artificial gene orderings or rely on shallow neural network architectures. We introduce a scalable latent diffusion model for single-cell gene expression data, which we refer to as scLDM, that respects the fundamental exchangeability property of the data. Our VAE uses fixed-size latent variables leveraging a unified Multi-head Cross-Attention Block (MCAB) architecture, which serves dual roles: permutation-invariant pooling in the encoder and permutation-equivariant unpooling in the decoder. We enhance this framework by replacing the Gaussian prior with a latent diffusion model using Diffusion Transformers and linear interpolants, enabling high-quality generation with multi-conditional classifier-free guidance. We show its superior performance in a variety of experiments for both observational and perturbational single-cell data, as well as downstream tasks like cell-level classification.

## 1 Introduction

Single-cell transcriptomics has revolutionized our understanding of cellular heterogeneity and biological processes at unprecedented resolution [1], enabling high-throughput gene expression profiling across millions of cells [2], and providing insights into cellular differentiation [3], disease progression [4], responses to drug perturbations [5–7]. However, modeling the complex, high-dimensional gene expression data from single cells presents significant computational and methodological challenges [8–10].

Deep generative modeling [11] offers a powerful framework to formulate expressive probability distributions. In the context of single-cell data, multiple methods have been proposed. In particular, Variational Auto-Encoders (VAEs) have been extensively utilized for representation learning (single-cell Variational Inference; scVI) [12], perturbation modeling [13, 14], trajectory inference [15], among others [16]. Additionally, Generative Adversarial Networks (GANs) have also been proposed, both for generating realistic cell populations (scGAN; [17]) and for inferring cellular trajectories [18]. Recently, diffusion-based models have also been adopted for single-cell gene expression [19]. An interesting research line was proposed in [20] that combines scVI with a flow matching model in the latent space (CFGGen).

However, two key challenges limit existing methods. First, they often require a fixed ordering of genes or operate on a restricted subset of highly variable genes (HGVs). This assumption directly clashes with the biological reality that gene expression profiles are **exchangeable** sets, where the order of genes carries no meaning. Second, approaches based on GANs inherit well-known training instabilities and risks of mode collapse. These limitations make current models inflexible, difficult to scale, and unable to properly handle the unordered nature of single-cell data.

<sup>‡</sup> Contact: Giovanni Palla (gpalla@chanzuckerberg.com), Theofanis Karaletsos (tkaraletsos@chanzuckerberg.com), Jakub M. Tomczak (jtomczak@chanzuckerberg.com)

\* Co-last authors

© 2025 The authors



This work is licensed under Creative Commons Attribution 4.0 International license (CC-BY).

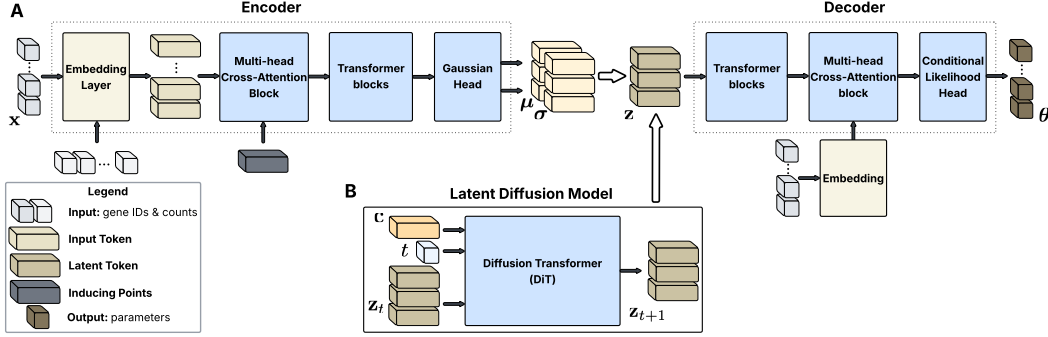


FIGURE 1. Our deep generative model, scLDM, for single-cell gene expression data. **A:** A fully transformer-based architecture for processing gene expressions. The encoder network results in permutation-invariant latent variables represented as tokens. The decoder network returns permutation-equivariant counts for given gene IDs. **B:** At the second stage, a vanilla prior is replaced by a latent diffusion model. We model latent tokens using Diffusion Transformers (DiT), and train the resulting LDM using linear interpolants and the flow matching loss. Sampling is carried out by applying the Scalable Interpolant Transformers (SiT) library [21].

This paper introduces a novel approach that combines the flexibility of VAEs with the power of latent diffusion models (see Figure 1), specifically designed to handle the exchangeable nature of gene expression data. The key insight is that careful architectural choices, particularly in the parameterization of permutation-invariant and permutation-equivariant components, result in a scalable, deep, and exchangeable generative model. The contributions of the paper are the following:

- We propose a novel fully transformer-based VAE architecture for exchangeable data that uses a single set of fixed-size, permutation-invariant latent variables. The model introduces a Multi-head Cross-Attention Block (MCAB) that serves dual purposes: It acts as a permutation-invariant pooling operator in the encoder, and functions as a permutation-equivariant unpooling operator in the decoder. This unified approach eliminates the need for separate architectural components for handling varying set sizes.
- We replace the standard Gaussian prior with a latent diffusion model trained with the flow matching loss and linear interpolants using the Scalable Interpolant Transformers formulation (SiT) [21], and a denoiser parameterized by Diffusion Transformers (DiT) [22]. This allows for better modeling of the complex distribution of cellular states and enables controlled generation through classifier-free guidance.
- The proposed framework, which we refer to as scLDM, supports generation conditioned on multiple attributes simultaneously through an extended classifier-free guidance mechanism, enabling fine-grained control over generated cell states, as demonstrated on multiple benchmark datasets. Moreover, we indicate the strengths of our fully transformer-based auto-encoder in terms of reconstruction metrics and on a downstream prediction task.

## 2 Background

**Variational Auto-Encoders** Another approach is Variational Auto-Encoders [23, 24], which offer flexible modeling capabilities. [25] proposed SetVAE with two latent variables for varying set sizes:  $\mathbf{z}_j$  matching  $\mathbf{x}_j$ 's dimensionality (where  $\mathbf{z}_i$  corresponds to  $\mathbf{x}_i$ ,  $i \in \mathcal{J}$ ) and constant-size  $\mathbf{c} \in \mathbb{R}^{d_1}$ . They used hierarchical VAE with multiple  $\mathbf{z}_j$  and  $\mathbf{c}$  layers and replaced conditional likelihood with Chamfer Distance. While we appreciate VAE's flexibility, we find two distinct latents and hierarchical structure unnecessary, arguing that careful parameterization is *crucial* for high performance.

**Permutation-equivariant/invariant Parameterizations** Geometric deep neural networks typically compose permutation-invariant and/or permutation-equivariant layers with nonlinearity activations [26]. DeepSets [27] exemplifies this blueprint by processing elements consistently regardless of position, then

applying symmetric aggregation (averaging or pooling [28–30]) to ensure permutation invariance. However, processing elements separately before aggregation with non-learnable pooling is limiting. Learned attention mechanisms in transformer architectures offer a solution, enabling joint element transformation. SetTransformer [31] introduces multi-head attention blocks and Pooling by Multi-head Attention for permutation invariance. We propose an alternative parameterization using a single multi-head attention layer for fixed-size output, followed by transformer blocks.

**Latent Diffusion Models** Latent Diffusion Models (LDMs) perform diffusion processes in learned latent spaces rather than directly in high-dimensional data spaces. Stable Diffusion [32] pioneered this approach for text-to-image synthesis by training diffusion models in the latent space of a pre-trained VAE, dramatically reducing computational costs while maintaining generation quality. This paradigm has proven effective across diverse scientific domains: all-atom diffusion transformers [33] generate molecules and materials with atomic-level precision, similarly LaM-SLidE [34] utilizes transformer-based LDM for molecular dynamics (among others), while La-proteina [35] employs transformer-based partially latent flow matching for atomistic protein generation. These advances demonstrate the versatility of latent diffusion approaches for complex, high-dimensional scientific data across multiple modalities. Here, we extend this framework to single-cell transcriptomics by proposing a transformer-based LDM for this biological data type.

**Generative Models for scRNA-seq** In the context of single-cell genomics, numerous generative models have been developed for (conditional) sampling of gene expression profiles. scVI [12] represents an early VAE-based generative model, while more recent approaches include GAN-based and diffusion-based architectures such as scGAN [36] and scDiffusion [19]. These models operate in continuous space and therefore transform discrete gene expression data into log-normalized counts. Recently, latent diffusion frameworks have emerged with models like SCLD [37] and CFGen [20], which leverage latent diffusion frameworks. Additionally, application-specific generative models have been developed for perturbational single-cell genomics, including CPA [38], SquiDiff [39], CellFlow [40], and CellOT [41], which are tailored to capture the effects of genetic and chemical perturbations on cellular states. Our approach is similar in vein to CFGen and SCLD, but leverages transformer-based architectures for both our newly proposed VAE as well as the latent diffusion model.

## 3 Methodology

### 3.1 Problem formulation

Let us consider  $M$  random variables,  $\mathbf{x}$ , where each  $\mathbf{x}_i \in \mathbb{X}^D$ , e.g.,  $\mathbb{X} = \mathbb{N}$ . A set of indices of  $M$  random variables is denoted as  $\mathcal{J}$ , namely,  $\mathcal{J} = \pi(\{1, 2, \dots, M\})$ , where  $\pi(\cdot)$  is a permutation<sup>1</sup>. Further, we denote a specific order of variables in  $\mathbf{x}$  determined by  $\mathcal{J}$  as  $\mathbf{x}_{\mathcal{J}}$ . We assume that for a given  $\mathcal{J}$ , an object  $\mathbf{x}_{\mathcal{J}}$  is equivalent to an object defined by  $\pi(\mathcal{J})$ , namely,  $\mathbf{x}_{\mathcal{J}} = \mathbf{x}_{\pi(\mathcal{J})}$ . An example of such a setting is gene expression data where  $\{1, 2, \dots, M\}$  corresponds to gene IDs and the order of gene IDs does not change the state of a cell. Further, we assume a *true* conditional distribution model  $p(\mathbf{x}_{\mathcal{J}}|\mathcal{J})$  that for a given order of indices  $\mathcal{J}$  allows sampling  $\mathbf{x}_{\mathcal{J}}$ . We access this *true* distribution through observed *iid* data  $\mathcal{D} = \{(\mathbf{x}_{j_n}, \mathcal{J}_n)\}_{n=1}^N$ . We look for a model  $p(\mathbf{x}_{\mathcal{J}}|\theta, \mathcal{J})$  with parameters  $\theta$  that optimizes the log-likelihood function for the empirical distribution with data  $\mathcal{D}$ ,  $\ell(\theta; \mathcal{D}) = \sum_{n=1}^N \ln p(\mathbf{x}_{j_n}|\theta, \mathcal{J}_n)$ . Moreover, we are interested in finding a single model that for given indices  $\mathcal{J}$  generates corresponding  $\mathbf{x}_{\mathcal{J}}$ . Formally, we require the model to be *exchangeable*, namely,  $p(\mathbf{x}_{\mathcal{J}}|\mathcal{J}) = p(\mathbf{x}_{\pi(\mathcal{J})}|\pi(\mathcal{J}))$ . For instance, a model generates the same gene expression profile for given different orders of gene IDs.

To model an exchangeable probabilistic model  $p(\mathbf{x}_{\mathcal{J}}|\theta, \mathcal{J})$ , we introduce  $m$  latent variables (i.e., the number of latents is fixed for all subsets  $\mathcal{J}$ ),  $\mathbf{Z} \in \mathbb{R}^{m \times D}$ . By using the family of variational posteriors of the form  $q(\mathbf{Z}|\phi, \mathbf{x}_{\mathcal{J}})$ , the Evidence Lower Bound (ELBO) is the following:

$$\ln p(\mathbf{x}_{\mathcal{J}}|\theta, \mathcal{J}) \geq \mathbb{E}_{\mathbf{Z} \sim q(\mathbf{Z}|\phi, \mathbf{x}_{\mathcal{J}})} [\ln p(\mathbf{x}_{\mathcal{J}}|\eta, \mathbf{Z}, \mathcal{J}) + \ln p(\mathbf{Z}|\psi) - \ln q(\mathbf{Z}|\phi, \mathbf{x}_{\mathcal{J}})], \quad (1)$$

<sup>1</sup>We denote a permutation either as a function  $\pi(\cdot)$  or, equivalently, as a matrix  $\mathbf{P}$ .

where  $\theta = \{\eta, \psi, \phi\}$  are the parameters of the model. We propose to model these parameters using neural networks, namely:  $\phi(\mathbf{x}_j) = \text{NN}_{enc}(\mathbf{x}_j)$ ,  $\eta(\mathbf{Z}, \mathcal{J}) = \text{NN}_{dec}(\mathbf{Z}, \mathcal{J})$ , and  $\psi$  are weights of a parameterization of the prior. Since our assumption is that the model must be exchangeable, we propose to parameterize the distributions in a way that: (i)  $\mathbf{Z}$  is permutation-invariant, namely, we aim for defining variational posteriors as Gaussian distributions with permutation-invariant neural networks  $\text{NN}_{enc}$ , (ii) the conditional likelihood is defined as  $p(\mathbf{x}_j|\eta(\mathbf{Z}, \mathcal{J})) = \prod_{i \in \mathcal{I}} p(\mathbf{x}_i|\eta_i(\mathbf{Z}, \mathcal{J}))$ , hence, we must ensure that:  $\mathbf{P}\eta(\mathbf{Z}, \pi(\mathcal{J})) = \text{NN}(\mathbf{Z}, \pi(\mathcal{J}))$ .

### 3.2 scLDM: A Transformer-based VAE with Latent Diffusion

**Permutation-invariant/equivariant Cross-Attention** Our VAE is parameterized by a novel transformer-based architecture that leverages multi-head cross-attention block (MCAB), enabling pooling/unpooling operations to avoid processing tens of thousands of tokens at the same time:

$$\text{MCAB}_{\mathcal{S}}(\mathbf{X}) = F(\mathbf{X}, \mathbf{S}) + \text{MLP}(\text{LN}_F(F(\mathbf{X}, \mathbf{S}))) \quad (2)$$

$$F(\mathbf{X}, \mathbf{S}) = \mathbf{Q} + \text{Att}_K(\text{LN}_Q(\mathbf{Q}), \mathbf{K}, \mathbf{V}) \quad (3)$$

$$\mathbf{Q} = \text{Linear}_{\mathcal{S}}(\mathbf{S}), \mathbf{K} = \text{Linear}_K(\text{LN}_K(\mathbf{X})), \mathbf{V} = \text{Linear}_V(\text{LN}_V(\mathbf{X})), \quad (4)$$

where Linear is a linear layer,  $\text{LN}(\cdot)$  denotes a layer norm, and  $\text{MLP}(\cdot)$  is a small fully-connected neural network, e.g.,  $\text{MLP}(\mathbf{X}) = (\text{Linear} \circ (\text{Linear} \odot (\text{silu} \circ \text{Linear}))) (\mathbf{X})$ .<sup>2</sup>  $\mathbf{S}$  are learnable pseudoinputs.  $\text{MCAB}_{\mathcal{S}}$  is defined similarly to a block used in Perceiver [42, 43].

MCAB is either permutation-invariant or permutation-equivariant. Since it relies on the attention mechanism, if we permute  $\mathbf{X}$  but do not permute  $\mathbf{S}$ , then MCAB is permutation-invariant (see Property 3 for the proof). However, if we process  $\mathbf{Z}$  by a permutation-invariant function and we permute  $\mathbf{S}$  accordingly to the permuted indices, then MCAB becomes permutation-equivariant (see Property 4 for the proof). As a result, we use MCAB as a permutation-invariant pooling operator in the encoder network, and as a permutation-equivariant unpooling operator in the decoder network.

**Encoder (Variational Posterior)** We define the family of variational posteriors as Gaussians,  $q(\mathbf{Z}|\phi(\mathbf{x}_j)) = \mathcal{N}(\mathbf{Z}|\mu(\mathbf{x}_j), \sigma(\mathbf{x}_j))$ ,  $\phi(\mathbf{x}_j) \stackrel{df}{=} \{\mu(\mathbf{x}_j), \sigma^2(\mathbf{x}_j)\}$ . We need  $\mathbf{Z}$  to be of fixed size and invariant to permutations of  $\mathbf{x}_j$ , we propose the following architecture of the encoder network:

$$\text{NN}_{enc}(\mathbf{x}_j, \mathcal{J}) = (\text{T}_L \circ \text{T}_{L-1} \circ \dots \circ \text{T}_1 \circ \text{MSCAB}_{\mathcal{S}} \circ \text{Embedding})(\mathbf{x}_j, \mathcal{J}), \quad (5)$$

where  $\text{T}_l(\cdot)$  denotes a transformer block, e.g.,  $\text{T}_l(\mathbf{X}) = ((\text{Id} \oplus (\text{MLP} \circ \text{LN}_2)) \circ (\text{Id} \oplus (\text{Att}_K \circ \text{LN}_1))) (\mathbf{X})$ , and  $\text{Embedding}(\cdot, \cdot)$  is an embedding layer. Since inputs  $\mathbf{x}_j$  form a (column) vector of counts, and  $\mathcal{J}$  are IDs, we propose to use the following embedding layer:

$$\text{Embedding}(\mathbf{x}_j, \mathcal{J}) = \text{Linear} \circ (\text{repeat}_D(\mathbf{x}_j) \boxplus \mathbf{E}_{\mathcal{J}}), \quad (6)$$

where  $\text{repeat}_D$  repeats the counts  $D$ -times resulting in a matrix  $M \times D$ , Linear projects the concatenated  $2D$ -dimensional space to the  $D$ -dimensional space, and  $\mathbf{E} \in \mathbb{R}^{M \times D}$  is the embedding matrix. The rationale behind this way of embedding both counts and indices is to mix the information and be able to learn the mixing through a projection layer. Additionally, we propose to encode only expressed genes, and replace non-expressed genes with a PAD token. We provide more details and an example in Appendix F.1.

The last transformer block duplicates the embedding dimension such that both the means  $\mu$  and the variances  $\sigma^2$  of a Gaussian are modeled. Alternatively, we can output means only to have an auto-encoder architecture, which is typically used in Latent Diffusion Models [32]. Note that all transformer blocks are permutation-equivariant, but our  $\text{MCAB}_{\mathcal{S}}$  is permutation-invariant. As a result, the proposed parameterization  $\text{NN}_{enc}$  results in permutation-invariant variational posteriors.

**Decoder (Conditional Likelihood)** The decoder network parameterizes the conditional likelihood function  $p(\mathbf{x}_j|\eta(\mathbf{Z}, \mathcal{J}))$  for given latents  $\mathbf{Z}$  and indices  $\mathcal{J}$ . The conditional likelihood could be a Gaussian if  $\mathbf{x}$ 's are continuous, or Poisson or Negative Binomial for counts. To fulfill the requirement on modeling

<sup>2</sup>We use the following notation for function compositions:  $(f \circ g)(x) \stackrel{df}{=} f(g(x))$ ,  $(f \cdot g)(x) \stackrel{df}{=} f(x)g(x)$ ,  $(f \oplus g)(x) \stackrel{df}{=} f(x) + g(x)$ , and  $(f \boxplus g)(x) \stackrel{df}{=} \text{concatenate}(f(x), g(x))$ .

exchangeable distributions, we need to ensure the conditional likelihood is exchangeable. In other words, for a given permutation  $\pi$ , the following holds true:  $p(\mathbf{x}_J|\eta(\mathbf{Z}, \mathcal{J})) = p(\mathbf{x}_{\pi(\mathcal{J})}|\eta(\mathbf{Z}, \pi(\mathcal{J})))$ . First, we assume that for given  $\mathbf{Z}$ , the conditional likelihood is fully factorized:  $p(\mathbf{x}_J|\eta(\mathbf{Z}, \mathcal{J})) = \prod_{i \in \mathcal{I}} p(\mathbf{x}_i|\eta_i(\mathbf{Z}, \mathcal{J}))$ . Next, we make the parameterization of  $p(\mathbf{x}_J|\eta(\mathbf{Z}, \mathcal{J}))$  permutation equivariant, because, otherwise, transforming  $\mathbf{Z}$  would result in incorrect parameters for each component  $p(\mathbf{x}_i|\eta_i(\mathbf{Z}, \mathcal{J}))$ . Keeping in mind that  $\mathbf{Z}$  is permutation-invariant to permutations of  $\mathbf{x}_J$ , we propose the following decoder network:

$$\text{NN}_{dec}(\mathbf{Z}, \mathcal{J}) = (\text{MCAB}_{\mathbf{E}_J} \circ \text{T}_L \circ \dots \circ \text{T}_1)(\mathbf{Z}, \mathcal{J}), \quad (7)$$

and then use the outcomes of  $\text{NN}_{dec}(\mathbf{Z}, \mathcal{J})$  to parameterize an appropriate distribution, e.g., the Negative Binomial (see Appendix F.2 for further details).

In our decoder network, we use  $\text{MCAB}_{\mathbf{E}_J}$  as our final block that outputs the parameters of the conditional likelihood. To make sure the model is permutation-equivariant, we define pseudoinputs in the multi-head cross-attention block selecting embedding vectors specified by  $\mathcal{J}$ ,  $\mathbf{S} = \mathbf{E}_J$ , where  $\mathbf{E}$  is the embedding used in the encoder network. This way, we ensure permutation-equivariance since permuting indices is equivalent to permuting embedding vectors,  $\mathbf{E}_{\pi(\mathcal{J})} = \mathbf{E}_J$ , see Property 4 in Appendix. Eventually, we obtain a family of exchangeable conditional likelihood functions.

**Prior (Marginal over Latents)** The final component of the proposed VAE is the *prior* of latent variables. Formulating permutation-equivariant priors is challenging [44]; fortunately, our latents  $\mathbf{Z}$  are permutation-invariant and length-invariant. As a result, we can use any prior distribution we prefer, including standard Gaussian,  $p(\mathbf{Z}) = \mathcal{N}(\mathbf{Z}|\mathbf{0}, \mathbf{I})$ .

In this paper, we advocate to use a Latent Diffusion Model (LDM) [32], namely, for a pre-trained VAE, we fit a diffusion-based model in the latent space to replace a *simpler* prior like  $\mathcal{N}(\mathbf{Z}|\mathbf{0}, \mathbf{I})$ . Using LDMs not only results in a better match with the aggregated posterior [11, 45], but allows the application of controlled sampling using techniques such as classifier-free guidance [46]. In particular, we focus on linear interpolants and the flow matching (FM) loss [47, 48], and the following version of the classifier-free guidance for FM:

$$\tilde{v}_{t,\epsilon}(\mathbf{Z}, y) = v_{t,\epsilon}(\mathbf{Z}; \text{Null}) + \omega [v_{t,\epsilon}(\mathbf{Z}; y) - v_{t,\epsilon}(\mathbf{Z}; \text{Null})], \quad (8)$$

where  $v_{t,\epsilon}(\mathbf{Z}; \cdot)$  is a parameterized vector field, and  $\omega$  is the guidance strength for attributes  $y \in \{0, 1\}^J$ , where any combination of attributes is possible (we refer to it as *joint conditioning*); the Null attribute corresponds to no conditioning. In CFGen [20], a different classifier-free guidance was used, namely,  $\tilde{v}_{t,\epsilon}(\mathbf{Z}, y) = v_{t,\epsilon}(\mathbf{Z}; \text{Null}) + \sum_{j=1}^J \omega_j [v_{t,\epsilon}(\mathbf{Z}; y_j) - v_{t,\epsilon}(\mathbf{Z}; \text{Null})]$ , that assumes *additive conditioning* s.t.  $\sum_j y_j = 1$ .

We parameterize the vector field (score) model using Diffusion Transformer (DiT) blocks [22]. The network is a composition of DiT and perfectly fits our modeling scenario since latents  $\mathbf{Z}$  are tokens.

### 3.3 Training & Sampling

**Training** We train our model (scLDM) using the two-stage approach: (1) A VAE is trained to learn a permutation-invariant latent space by reconstructing subsets of variables; and (2) An LDM is trained to generate new samples from this latent space which can be controlled by classifier-free guidance [46] with multiple conditions [20].

*Stage 1: VAE* We train our VAE with a standard Gaussian prior by optimizing the ELBO in (1). However, to encourage better reconstruction capabilities, we introduce  $\beta$ -weighting of the KL-term like in [49]. In the most extreme case, we set  $\beta$  to 0 and the encoder returns means only,  $\mu(\mathbf{x}_J)$ .

*Stage 2: LDM* In the second stage, we freeze the VAE and replace the standard Gaussian prior with a score-based (diffusion) model parameterized by a DiT network trained with linear interpolants and the flow matching loss. Additionally, to encourage controlled sampling, for each element of a mini-batch, we sample from the Bernoulli distribution with probability  $\rho$  to determine whether conditioning is used or not.

**Sampling** In our model, sampling  $\mathbf{x}$ 's determined by the indices  $\mathcal{J}$  is defined by the following generative process: (i)  $\mathbf{Z} \sim p(\mathbf{Z})$ , (ii)  $\mathbf{x}_J \sim p(\mathbf{x}_J|\eta(\mathbf{Z}, \mathcal{J}))$ . We can also sample *conditionally* by applying the classifier-free guided sampling technique, following the vector field defined in (39).

## 4 Experiments

**Settings** We provide more details on the experiments in the Appendix, namely, the datasets in Appendix G, the baselines in Appendix H, the hyperparams of our scLDM in Appendix I, the evaluation pipeline with metrics in Appendix J, and additional results in Appendix L. In the following experiments, we present superior capabilities of our scLDM: (i) the powerful reconstructive performance of the fully transformer-based VAE, (ii) the unconditional and conditional generative performance on observational and perturbational datasets, (iii) the usefulness of the embeddings provided by our auto-encoder on classification downstream tasks.

### 4.1 (Un)conditional Cell Generation on Observational Data

**Details** For the first experiment, we used single-cell RNA-sequencing data from the benchmark datasets used in [20]. Here, we are interested in evaluating the reconstructive and generative capabilities of our scLDM. For generations, we train our scLDM to synthesize gene expression profiles conditioned on a single attribute. At inference time, we query the model with specific labels to generate new synthetic cells that match the desired cellular identity. In the case of unconditional generation, we sample from the vector field without conditioning on the cell type label (i.e.,  $y = \text{Null}$ ). We compare our approach to scVI [12], scDiffusion [19], and the current SOTA generative model CFGen [20].

TABLE 1. Model performance comparison on cell reconstruction task.

Dataset	Model	RE ↓	PCC ↑	MSE ↓
Dentate Gyrus	scVI	<b>5193.2</b> ± 0.1	0.058 ± 0.000	0.378 ± 0.000
	CFGen	5468.8 ± N/A	0.076 ± N/A	0.253 ± N/A
	scLDM	<b>5232.9</b> ± 43.1	<b>0.103</b> ± 0.005	<b>0.249</b> ± 0.002
Tabula Muris	scVI	5588.2 ± 1.7	0.221 ± 0.000	0.132 ± 0.000
	CFGen	5547.6 ± N/A	0.136 ± N/A	0.127 ± N/A
	scLDM	<b>4569.6</b> ± 105.1	<b>0.391</b> ± 0.021	<b>0.092</b> ± 0.004
HLCA	scVI	5659.2 ± 0.5	0.125 ± 0.000	0.238 ± 0.000
	CFGen	5428.7 ± N/A	0.146 ± N/A	0.117 ± N/A
	scLDM	<b>4102.1</b> ± 41.1	<b>0.421</b> ± 0.013	<b>0.069</b> ± 0.001

**Results and discussion** Our proposed scLDM model demonstrates substantial improvements over existing approaches across all evaluated datasets and metrics, see Table 1. scLDM consistently achieves the lowest reconstruction error values, with particularly notable improvements on Tabula Muris (4569.6 vs. 5547.6 for CFGen) and HLCA (4102.1 vs. 5428.7 for CFGen) datasets. The Pearson correlation coefficients show dramatic improvements, with scLDM achieving 0.391 on Tabula Muris compared to 0.221 for scVI and 0.136 for CFGen, nearly doubling the correlation with ground truth. Similarly, MSE is consistently reduced, with scLDM achieving 0.069 on HLCA compared to 0.117 for CFGen and 0.238 for scVI. These results suggest that our fully transformer-based VAE is able to more effectively capture the complex structure of single-cell gene expression data compared to traditional VAE-based methods (scVI, CFGen). The consistent improvements across diverse tissue types (brain, entire organism, and lung) indicate the generalizability of our approach, namely, a parameterization of the VAE using the proposed transformer-based architectures.

Table 2 presents the generation benchmarks, where scLDM demonstrates superior performance across both unconditional and conditional generation sampling. In the unconditional setting, our model achieves the lowest Wasserstein-2 distance across all datasets, with improvements ranging from 14% on Dentate Gyrus to 12% on Tabula Muris. While CFGen shows competitive performance on MMD<sup>2</sup> RBF, our approach matches or outperforms it, achieving identical scores on HLCA and superior results on Tabula Muris. In terms of the Fréchet Distance (FD), scLDM still shows superior performance, with particularly striking improvements on Tabula Muris, where it achieves a nearly three-fold reduction compared to the second-best baseline. For conditional generation, scLDM maintains its performance edge with consistent improvements

TABLE 2. Model performance comparison on (un)conditional cell generation benchmarks on highly variable genes.

Setting	Model	W2 ↓	MMD <sup>2</sup> RBF ↓	FD ↓
Dentate Gyrus				
Uncond	scDiffusion	17.443 ± 0.028	0.258 ± 0.002	256.630 ± 0.357
	CFGen	12.617 ± 0.034	<b>0.022</b> ± 0.001	<b>28.105</b> ± 0.332
	scLDM	<b>10.817</b> ± 0.065	<b>0.023</b> ± 0.000	28.403 ± 0.099
Cond	scDiffusion	17.321 ± 0.041	0.689 ± 0.000	261.217 ± 1.856
	CFGen	11.608 ± 0.066	<b>0.075</b> ± 0.000	41.425 ± 1.612
	scLDM	<b>10.615</b> ± 0.028	0.102 ± 0.003	<b>34.388</b> ± 1.014
Tabula Muris				
Uncond	scDiffusion	14.143 ± 0.007	0.144 ± 0.001	158.977 ± 1.070
	CFGen	11.658 ± 0.127	0.008 ± 0.000	36.373 ± 1.165
	scLDM	<b>10.295</b> ± 0.110	<b>0.004</b> ± 0.000	<b>13.130</b> ± 0.318
Cond	scDiffusion	14.143 ± 0.007	0.144 ± 0.001	158.977 ± 1.070
	CFGen	8.921 ± 0.034	0.026 ± 0.000	21.517 ± 0.596
	scLDM	<b>7.717</b> ± 0.030	<b>0.016</b> ± 0.000	<b>11.008</b> ± 0.716
HLCA				
Uncond	scDiffusion	15.886 ± 0.038	0.163 ± 0.001	210.853 ± 1.165
	CFGen	12.433 ± 0.045	<b>0.007</b> ± 0.000	24.639 ± 0.738
	scLDM	<b>10.419</b> ± 0.079	<b>0.007</b> ± 0.000	<b>18.024</b> ± 0.372
Cond	scDiffusion	15.886 ± 0.038	0.163 ± 0.001	210.853 ± 1.165
	CFGen	9.757 ± 0.078	0.090 ± 0.006	33.900 ± 5.116
	scLDM	<b>8.445</b> ± 0.045	<b>0.074</b> ± 0.002	<b>20.974</b> ± 1.504

in W2, MMD<sup>2</sup> RBF, and FD scores across all datasets. We report further generation results on all genes in Appendix. In Figure 2 we report qualitative evaluations of generation results for the HLCA datasets for all three models. Our model shows qualitatively a better coverage of the cell state variation on UMAP coordinates, showcasing how it is able to recapitulate high resolution cell states in highly heterogenous tissues like the human lung. Additionally, in Appendix L.2 we provide an interpretability analysis on the cross-attention scores of the encoder-decoder model of scLDM, showing how the latent tokens map to specific marker gene set patterns. These results demonstrate that our latent diffusion approach not only generates more realistic single-cell expression profiles but also maintains superior performance when conditioning on cell state information, a crucial capability for practical applications in single-cell genomics.

## 4.2 Conditional Cell Generation on Perturbational Data

**Details** In the second experiment, we train our model for conditional gene expression generation based on multiple attributes: a cell context (cell lines and cell types) and a perturbation type (gene knockouts and cytokines). The VAE baseline is trained without attribute conditioning, focusing solely on the reconstruction objective, while the flow matching component incorporates multi-attribute conditioning. By training across diverse contexts, the model learns to capture joint structure spanning different axes of variation. At inference time, the flow matching model is queried with specific combinations of cell type and perturbation to generate new gene expression profiles.

We leverage two datasets: (1) Parse 1M, containing perturbational single-cell RNA-sequencing data from human peripheral blood mononuclear cells (PBMCs) generated by Parse Biosciences [50] with 1,267,690 single cells across 18 annotated cell types, each subjected to one of 90 cytokine perturbations or a control condition, and to test generalization capabilities, we hold out 27 cytokine perturbations in CD4 Naive cells; and (2) Replogle, a benchmark genetic perturbation dataset [51] consisting of 2,024 gene knockouts across four cell lines after filtering perturbations with low on-target efficacy Adduri et al. [5], holding out 372

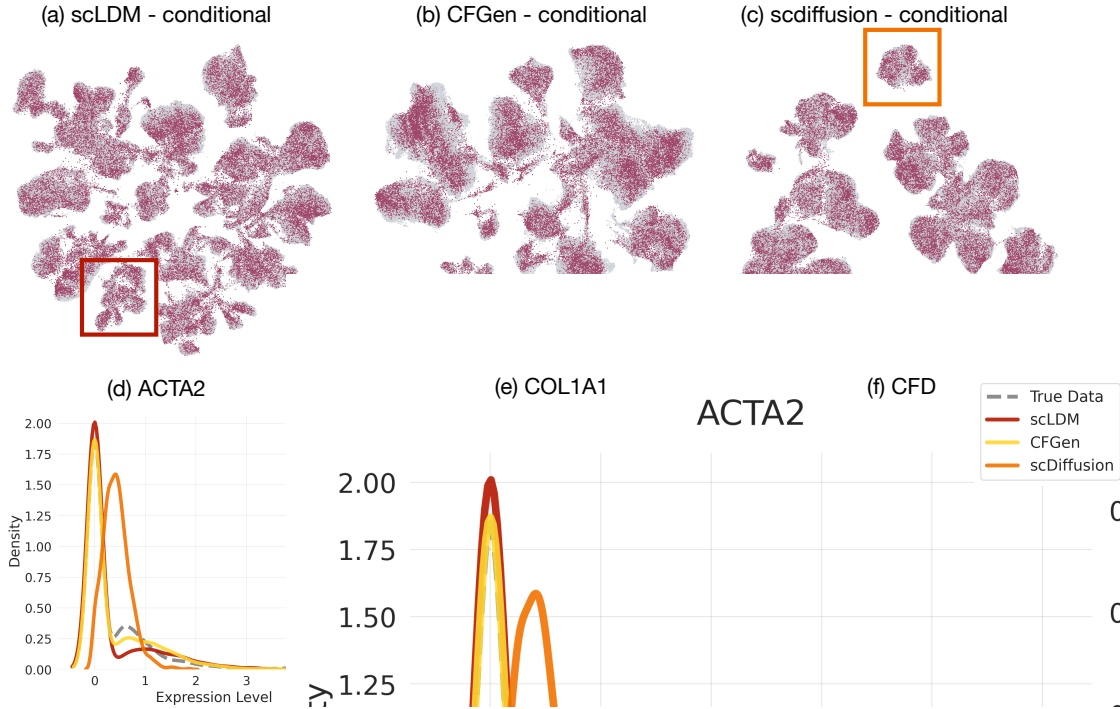


FIGURE 2. Conditional generation for the HLCA dataset for: (a) scLDM, (b) CFGen and (c) scdiffusion. Expression levels for 3 marker genes: (d) ACTA2, (e) COL1A1 and (f) CFD, markers of “alveolar type 2 fibroblast cell”, corresponding to cell populations in the insets.

TABLE 3. Model performance comparison on conditional cell generation on Parse1M and Replogle. For scLDM, we evaluated the generation performance across 3 different guidance weights ( $\omega$ )

Dataset	Model	W2 ↓	MMD <sup>2</sup> RBF ↓	FD ↓
Parse 1M	scVI	35.508 ± 0.182	1.372 ± 0.016	1233.109 ± 12.694
	CPA	13.534 ± 0.036	1.117 ± 0.014	181.324 ± 0.985
	scGPT	22.870 ± 0.152	2.203 ± 0.013	523.932 ± 7.043
	STATE	19.111 ± 0.136	0.714 ± 0.009	312.344 ± 5.743
	scLDM ( $\omega=1$ )	<b>12.457</b> ± 0.045	<b>0.027</b> ± 0.002	<b>18.136</b> ± 0.903
	scLDM ( $\omega=5$ )	12.902 ± 0.087	0.071 ± 0.004	43.363 ± 2.246
	scLDM ( $\omega=10$ )	13.638 ± 0.111	0.122 ± 0.006	69.769 ± 3.363
Replogle	scVI	17.359 ± 0.051	0.453 ± 0.003	284.474 ± 1.825
	CPA	11.510 ± 0.029	0.532 ± 0.003	126.805 ± 0.693
	scGPT	34.166 ± 0.272	3.087 ± 0.010	1247.679 ± 20.245
	STATE	20.58 ± 0.039	0.730 ± 0.003	366.642 ± 1.547
	scLDM ( $\omega=1$ )	<b>11.292</b> ± 0.033	<b>0.200</b> ± 0.002	<b>53.750</b> ± 0.666
	scLDM ( $\omega=5$ )	12.900 ± 0.069	0.320 ± 0.004	105.365 ± 1.935
	scLDM ( $\omega=10$ )	14.911 ± 0.091	0.436 ± 0.005	166.877 ± 3.036

genetic perturbations in HepG2 cells to evaluate generalization to unseen cell context-perturbation pairs. For both datasets, we restricted analysis to the top 2,000 highly variable genes (HVGs) following Adduri et al. [5]. We compare our model against established baselines: CPA [38], scVI [12], scGPT [52] and STATE-Tx [5].

**Results and Discussion** The results presented in Table 3 demonstrate that our proposed approach significantly outperforms the baselines in both the Parse 1M dataset (cytokine perturbation) and the Replogle

dataset (gene knockouts). Our model scLDM is substantially better across all metrics, improving up to  $\sim 90\%$  for  $MMD^2$  RBF and FD for the Parse 1M dataset and  $\sim 60\%$  for  $MMD^2$  RBF and FD for the Replogle dataset. This demonstrates how our model outperforms others in capturing the full range of cellular variation in perturbation responses across unseen combinations of cell contexts and perturbations. In Appendix 13, we report four additional metrics on perturbation predictions in unseen context, using the `cell-eval` [5]. Our model is competitive, and sometimes outperforms the stronger baseline STATE-Tx across both datasets.

In Figure 3, we report a qualitative evaluation of our model generative performances for the Parse 1M dataset for unseen combinations of CD4-Naive cells with various cytokine perturbations such as IL-9 and LT-alpha1-beta2. Furthermore, we show the same for Replogle dataset for unseen combinations of HepG2 cells with PPP6c and ZDHHC7 gene edits.

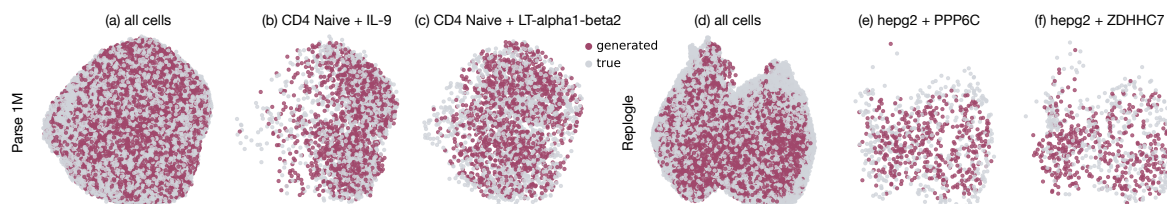


FIGURE 3. Conditional generation across multiple attributes: cell type and perturbation. (a) Generated vs. true cells across all cell types in the Parse 1M dataset show close alignment. (b–c) For CD4 Naive cells, conditioning on cytokine perturbations (IL-9, LT-alpha1-beta2) produces perturbation-specific shifts consistent with the true test distributions. (d) Generated vs. true cells across all cell types in the Replogle dataset. (e–f) For HepG2 cells, conditioning on genetic perturbations (PPP6C, ZDHHC7) yields realistic perturbation-dependent distributions that closely follow the experimental data.

In Appendix 15, we additionally report reconstruction results between the VAE component of scLDM and scVI for both datasets, showing how our improved transformer-based VAE significantly outperforms MLP-based scVI on the reconstruction task. Finally, we also tested how the additive conditioning for the classifier-free guidance proposed in [20] performs compared to the standard classifier-free guidance approach [46]. In Supplementary Table 15, we report that the standard approach is superior to the additive approach in multi-attribute conditional settings for perturbational single-cell data.

### 4.3 scLDM-VAE embedding evaluations on classification tasks

TABLE 4. COVID-19 model performance comparison (averaged across all donors). Since all standard errors are below 0.003 (see Appendix L.6), they are omitted in this table.

Model	F1 Score	Recall	Precision
TranscriptFormer	0.814	0.829	0.801
UCE	0.775	0.781	0.771
scGPT	0.779	0.793	0.766
Geneformer	0.768	0.781	0.757
AIDO.Cell	0.717	0.729	0.708
scVI	0.675	0.680	0.680
scLDM (20M)	0.811	0.827	0.797
scLDM (70M)	0.815	0.830	0.801
scLDM (270M)	<b>0.820</b>	<b>0.836</b>	<b>0.806</b>

**Details** For the third experiment, we leveraged two datasets: the first dataset is a human lung single-cell RNA-sequencing data from healthy donors and patients affected by COVID-19 [53], the second dataset

consists of 6 tissues from the Tabula Sapiens 2.0 [54]. The goal of this experiment is to verify the quality of embeddings provided by the auto-encoder on a downstream task (here: classification). We compare our approach to embeddings provided by TranscriptFormer [55], scVI [12], AIDO.Cell [56], Geneformer [57], scGPT [52], UCE [58]. We used Human Census data (CellxGene)<sup>3</sup> to train three versions of scLDM-VAE, namely, with around 20M parameters, 70M parameters, and 270M parameters. For our scLDM-VAE and benchmark models, both datasets represent out-of-distribution data that were unseen during training.

To evaluate the quality of the learned representations, we process each of the four COVID-19 donors through the models to generate cell embeddings. For scLDM variants, we use the mean of the latent distribution,  $\mu(\mathbf{x})$ , which is flattened to a 4096-dimensional vector. To ensure fair comparison across models with different embedding dimensions, we apply principal component analysis (PCA) to all embeddings, retaining the top 128 principal components. For each donor independently, we train an unregularized logistic regression classifier to distinguish infected from uninfected cells using 5-fold cross-validation. The final metrics are computed as equally weighted averages across the four donors, with uncertainties propagated using standard error addition in quadrature:  $\sigma_{\text{combined}} = \frac{1}{n} \sqrt{\sum_{i=1}^n \sigma_i^2}$ , where  $n = 4$  donors.

TABLE 5. Tabula Sapiens 2.0 model performance comparison (averaged across all tissues). Since all standard errors are below 0.003 (see Appendix L.6), they are omitted in this table.

Model	F1 Score	Recall	Precision
scGPT	0.8	0.802	0.806
scVI	0.799	0.794	0.814
TranscriptFormer	0.799	0.8	0.802
UCE	0.796	0.797	0.801
Geneformer	0.777	0.776	0.786
AIDO.Cell	0.724	0.715	0.748
scLDM (20M)	<b>0.804</b>	<b>0.805</b>	<b>0.812</b>
scLDM (70M)	0.802	0.802	0.810
scLDM (270M)	0.802	0.803	0.811

For the Tabula Sapiens 2.0 dataset, we evaluated cell type classification across 6 tissues: blood, spleen, lymph node, small intestine, thymus, and liver. Following the same protocol as the COVID-19 analysis, we stratified samples by tissue instead of donor and filtered out cell types with fewer than 100 cells to ensure robust classification. We employed multinomial logistic regression for the multi-class cell type prediction task. Final metrics are averaged over tissues with propagated uncertainties (see Appendix L.6).

**Results and discussion** As shown in Table 4, our 270M and 70M models achieve superior performance across all evaluated metrics for COVID-19 infection detection. The performance differences between scLDM (270M) and TranscriptFormer—the strongest benchmark model—represent meaningful differences given the measurement uncertainty, with our model achieving F1 score of  $0.820 \pm 0.001$  compared to TranscriptFormer’s  $0.814 \pm 0.002$ . The strong discriminative performance demonstrates that our transformer-based VAE learns biologically meaningful representations that capture infection-related transcriptional signatures. We observe substantial improvements over the VAE-based scVI model (F1:  $0.675 \pm 0.001$ ), highlighting the advantages of our architectural innovations and model scale.

For the Tabula Sapiens 2.0 classification results shown in Table 5, the differences in F1 scores between the scLDM model variants are within measurement uncertainty and may not be significant. Moreover, all top-performing models—scLDM variants, scGPT, scVI, and TranscriptFormer—achieve F1 scores within each other’s uncertainties (ranging from 0.799 to 0.804 with standard errors of 0.002), indicating comparable performance for multi-class cell type classification. The consistent performance across both binary (COVID-19 infection) and multi-class (cell type) classification tasks validates the biological utility of our learned embeddings, making them valuable for biological discovery applications beyond generation.

<sup>3</sup><https://cellxgene.cziscience.com/>

## 5 Conclusion

In this paper, we demonstrate that enforcing the inductive bias of exchangeability is crucial for the generative modeling of single-cell data. We introduced a scalable architecture that combines a permutation-invariant encoder and a permutation-equivariant decoder within a fully transformer-based VAE with a latent diffusion model parameterized using DiTs, achieving state-of-the-art performance on cell generation benchmarks, both observational and perturbational data, as well as downstream classification tasks. Our work extends beyond imposing artificial structure on gene expression data, instead providing a principled framework for learning from unordered sets. This approach is not limited to transcriptomics and lays the groundwork for developing foundational models for other exchangeable biological data, such as proteomics and epigenomics, as well as multi-omics and multi-modal data, thereby enabling more faithful and powerful virtual models of cellular biology.

### Author Contributions

GP: Conceptualization, Data curation, Formal analysis, Investigation, Methodology, Software, Validation, Visualization, Writing – review & editing, SB: Investigation, Software, Validation, Writing – review & editing, PD: Investigation, Software, Validation, Visualization, Writing – review & editing, DL: Project administration, AK: Supervision, Writing – review & editing, TK: Project administration, Conceptualization, Supervision, Writing – review & editing, JT: Conceptualization, Investigation, Methodology, Software, Supervision, Validation, Writing – original draft

### Acknowledgments

### References

- [1] Orit Rozenblatt-Rosen, Michael JT Stubbington, Aviv Regev, and Sarah A Teichmann. The Human Cell Atlas: from vision to reality. *Nature*, 550(7677):451–453, 2017.
- [2] Isaac Virshup, Danila Bredikhin, Lukas Heumos, Giovanni Palla, Gregor Sturm, Adam Gayoso, Iliia Kats, Mikaela Koutrouli, Bonnie Berger, et al. The scverse project provides a computational ecosystem for single-cell omics data analysis. *Nature biotechnology*, 41(5):604–606, 2023.
- [3] Gunsagar S Gulati, Shaheen S Sikandar, Daniel J Wesche, Anoop Manjunath, Anjan Bharadwaj, Mark J Berger, Francisco Ilagan, Angera H Kuo, Robert W Hsieh, Shang Cai, et al. Single-cell transcriptional diversity is a hallmark of developmental potential. *Science*, 367(6476):405, 2020.
- [4] Tao Zeng and Hao Dai. Single-cell rna sequencing-based computational analysis to describe disease heterogeneity. *Frontiers in Genetics*, 10:629, 2019.
- [5] Abhinav K Adduri, Dhruv Gautam, Beatrice Bevilacqua, Alishba Imran, Rohan Shah, Mohsen Naghipourfar, Noam Teyssier, Rajesh Ilango, Sanjay Nagaraj, Mingze Dong, et al. Predicting cellular responses to perturbation across diverse contexts with STATE. *bioRxiv*, pages 2025–06, 2025.
- [6] Michael Bereket and Theofanis Karaletsos. Modelling cellular perturbations with the sparse additive mechanism shift variational autoencoder. In *Neural Information Processing Systems*, 2023.
- [7] Jesse Zhang, Airol A Ubas, Richard de Borja, Valentine Svensson, Nicole Thomas, Neha Thakar, Ian Lai, Aidan Winters, Umair Khan, Matthew G Jones, et al. Tahoe-100m: A giga-scale single-cell perturbation atlas for context-dependent gene function and cellular modeling. *BioRxiv*, pages 2025–02, 2025.
- [8] David Lähnemann, Johannes Köster, Ewa Szczurek, Davis J McCarthy, Stephanie C Hicks, Mark D Robinson, Catalina A Vallejos, Kieran R Campbell, Niko Beerenwinkel, Ahmed Mahfouz, et al. Eleven grand challenges in single-cell data science. *Genome biology*, 21:1–35, 2020.
- [9] Malte D Luecken, Maren Büttner, Kridsakorn Chaichoompu, Anna Danese, Marta Interlandi, Michaela F Müller, Daniel C Strobl, Luke Zappia, Martin Dugas, Maria Colomé-Tatché, et al. Benchmarking atlas-level data integration in single-cell genomics. *Nature methods*, 19(1):41–50, 2022.

- [10] Karlynn E Neu, Qingming Tang, Patrick C Wilson, and Aly A Khan. Single-cell genomics: approaches and utility in immunology. *Trends in immunology*, 38(2):140–149, 2017.
- [11] Jakub M. Tomczak. *Deep Generative Modeling*. Springer International Publishing, 2024.
- [12] Romain Lopez, Jeffrey Regier, Michael B Cole, Michael I Jordan, and Nir Yosef. Deep generative modeling for single-cell transcriptomics. *Nature methods*, 15(12):1053–1058, 2018.
- [13] Mohammad Lotfollahi, Anna Klimovskaia Susmelj, Carlo De Donno, Leon Hetzel, Yuge Ji, Ignacio L Ibarra, Sanjay R Srivatsan, Mohsen Naghipourfar, Riza M Daza, Beth Martin, et al. Predicting cellular responses to complex perturbations in high-throughput screens. *Molecular systems biology*, 19(6): e11517, 2023.
- [14] Alessandro Palma, Fabian J Theis, and Mohammad Lotfollahi. Predicting cell morphological responses to perturbations using generative modeling. *Nature Communications*, 16(1):505, 2025.
- [15] Adam Gayoso, Philipp Weiler, Mohammad Lotfollahi, Dominik Klein, Justin Hong, Aaron Streets, Fabian J Theis, and Nir Yosef. Deep generative modeling of transcriptional dynamics for rna velocity analysis in single cells. *Nature Methods*, 21(1):50–59, 2024.
- [16] Adam Gayoso, Romain Lopez, Galen Xing, Pierre Boyeau, Valeh Valiollah Pour Amiri, Justin Hong, Katherine Wu, Michael Jayasuriya, Edouard Mehlman, Maxime Langevin, Yining Liu, Jules Samaran, Gabriel Misrachi, Achille Nazaret, Oscar Clivio, Chenling Xu, Tal Ashuach, Mariano Gabitto, Mohammad Lotfollahi, Valentine Svensson, Eduardo da Veiga Beltrame, Vitalii Kleshchevnikov, Carlos Talavera-López, Lior Pachter, Fabian J. Theis, Aaron Streets, Michael I. Jordan, Jeffrey Regier, and Nir Yosef. A python library for probabilistic analysis of single-cell omics data. *Nature Biotechnology*, Feb 2022. ISSN 1546-1696. doi: 10.1038/s41587-021-01206-w. URL <https://doi.org/10.1038/s41587-021-01206-w>.
- [17] Mohamed Marouf, Pierre Machart, Vikas Bansal, Christoph Kilian, Daniel S Magruder, Christian F Krebs, and Stefan Bonn. Realistic in silico generation and augmentation of single-cell rna-seq data using generative adversarial networks. *Nature communications*, 11(1):166, 2020.
- [18] Derek Reiman, Godhev Kumar Manakkat Vijay, Heping Xu, Andrew Sonin, Dianyu Chen, Nathan Salomonis, Harinder Singh, and Aly A Khan. Pseudocell tracer—a method for inferring dynamic trajectories using scrnaseq and its application to b cells undergoing immunoglobulin class switch recombination. *PLoS computational biology*, 17(5):e1008094, 2021.
- [19] Erpai Luo, Minsheng Hao, Lei Wei, and Xuegong Zhang. scdiffusion: conditional generation of high-quality single-cell data using diffusion model. *Bioinformatics*, 40(9), 2024.
- [20] Alessandro Palma, Till Richter, Hanyi Zhang, Manuel Lubetzki, Alexander Tong, Andrea Dittadi, and Fabian J Theis. Multi-modal and multi-attribute generation of single cells with cfgen. In *The Thirteenth International Conference on Learning Representations*, 2025.
- [21] Nanye Ma, Mark Goldstein, Michael S Albergo, Nicholas M Boffi, Eric Vanden-Eijnden, and Saining Xie. Sit: Exploring flow and diffusion-based generative models with scalable interpolant transformers. In *European Conference on Computer Vision*, pages 23–40. Springer, 2024.
- [22] William Peebles and Saining Xie. Scalable diffusion models with transformers. In *Proceedings of the IEEE/CVF international conference on computer vision*, pages 4195–4205, 2023.
- [23] Diederik P Kingma and Max Welling. Auto-encoding variational {Bayes}. In *Int. Conf. on Learning Representations*, 2014.
- [24] Danilo Jimenez Rezende, Shakir Mohamed, and Daan Wierstra. Stochastic backpropagation and approximate inference in deep generative models. In *International conference on machine learning*, pages 1278–1286. PMLR, 2014.
- [25] Jinwoo Kim, Jaehoon Yoo, Juho Lee, and Seunghoon Hong. Setvae: Learning hierarchical composition for generative modeling of set-structured data. In *Proceedings of the IEEE/CVF Conference on Computer Vision and Pattern Recognition*, pages 15059–15068, 2021.
- [26] Michael M Bronstein, Joan Bruna, Taco Cohen, and Petar Veličković. Geometric deep learning: Grids, groups, graphs, geodesics, and gauges. *arXiv preprint arXiv:2104.13478*, 2021.
- [27] Manzil Zaheer, Satwik Kottur, Siamak Ravanbakhsh, Barnabas Poczos, Russ R Salakhutdinov, and Alexander J Smola. Deep sets. *Advances in neural information processing systems*, 30, 2017.

- [28] Masanari Kimura, Ryotaro Shimizu, Yuki Hirakawa, Ryosuke Goto, and Yuki Saito. On permutation-invariant neural networks. *arXiv preprint arXiv:2403.17410*, 2024.
- [29] Maximilian Ilse, Jakub Tomczak, and Max Welling. Attention-based deep multiple instance learning. In *International conference on machine learning*, pages 2127–2136. PMLR, 2018.
- [30] Jiahao Xie and Guangmo Tong. Advances in set function learning: a survey of techniques and applications. *ACM Computing Surveys*, 57(7):1–37, 2025.
- [31] Juho Lee, Yoonho Lee, Jungtaek Kim, Adam Kosiorek, Seungjin Choi, and Yee Whye Teh. Set transformer: A framework for attention-based permutation-invariant neural networks. In *International conference on machine learning*, pages 3744–3753. PMLR, 2019.
- [32] Robin Rombach, Andreas Blattmann, Dominik Lorenz, Patrick Esser, and Björn Ommer. High-resolution image synthesis with latent diffusion models. In *Proceedings of the IEEE/CVF conference on computer vision and pattern recognition*, pages 10684–10695, 2022.
- [33] Chaitanya K Joshi, Xiang Fu, Yi-Lun Liao, Vahe Gharakhanyan, Benjamin Kurt Miller, Anuroop Sriram, and Zachary Ward Ulissi. All-atom Diffusion Transformers: Unified generative modelling of molecules and materials. In *Forty-second International Conference on Machine Learning*, 2025.
- [34] Florian Sestak, Artur Toshev, Andreas Fürst, Günter Klambauer, Andreas Mayr, and Johannes Brandstetter. LaM-SLidE: Latent Space Modeling of Spatial Dynamical Systems via Linked Entities. *arXiv preprint arXiv:2502.12128*, 2025.
- [35] Tomas Geffner, Kieran Didi, Zhonglin Cao, Danny Reidenbach, Zuobai Zhang, Christian Dallago, Emine Kucukbenli, Karsten Kreis, and Arash Vahdat. La-proteina: Atomistic protein generation via partially latent flow matching. *arXiv preprint arXiv:2507.09466*, 2025.
- [36] Matteo Marouf, Pierre Machart, Vikas Bansal, Christoph Kilian, Daniel S Magruder, Christian F Krebs, and Stefan Bonn. Realistic in silico generation and augmentation of single-cell RNA-seq data using generative adversarial networks. *Nat. Commun.*, 11(1):166, January 2020.
- [37] Yixuan Wang, Shuangyin Li, Shimin DI, and Lei Chen. Single-cell rna-seq synthesis with latent diffusion model, 2023. URL <https://arxiv.org/abs/2312.14220>.
- [38] Mohammad Lotfollahi, Anna Klimovskaia Susmelj, Carlo De Donno, Leon Hetzel, Yuge Ji, Ignacio L Ibarra, Sanjay R Srivatsan, Mohsen Naghipourfar, Riza M Daza, Beth Martin, Jay Shendure, Jose L McFaline-Figueroa, Pierre Boyeau, F Alexander Wolf, Nafissa Yakubova, Stephan Günemann, Cole Trapnell, David Lopez-Paz, and Fabian J Theis. Predicting cellular responses to complex perturbations in high-throughput screens. *Molecular Systems Biology*, 19(6):e11517, 2023. doi: <https://doi.org/10.15252/msb.202211517>. URL <https://www.embopress.org/doi/abs/10.15252/msb.202211517>.
- [39] Siyu He, Yuefei Zhu, Daniel Naveed Tavakol, Haotian Ye, Yeh-Hsing Lao, Zixian Zhu, Cong Xu, Shradha Chauhan, Guy Garty, Raju Tomer, et al. Squidiff: Predicting cellular development and responses to perturbations using a diffusion model. *bioRxiv*, pages 2024–11, 2024.
- [40] Dominik Klein, Jonas Simon Fleck, Daniil Bobrovskiy, Lea Zimmermann, Sören Becker, Alessandro Palma, Leander Dony, Alejandro Tejada-Lapuerta, Guillaume Hugué, Hsiu-Chuan Lin, Nadezhda Azbukina, Fátima Sanchís-Calleja, Theo Uscidda, Artur Szalata, Manuel Gander, Aviv Regev, Barbara Treutlein, J Gray Camp, and Fabian J Theis. CellFlow enables generative single-cell phenotype modeling with flow matching. April 2025.
- [41] Charlotte Bunne, Stefan G. Stark, Gabriele Gut, Jacobo Sarabia del Castillo, Mitch Levesque, Kjong-Van Lehmann, Lucas Pelkmans, Andreas Krause, and Gunnar Rätsch. Learning single-cell perturbation responses using neural optimal transport. *Nature Methods*, 20(11):1759–1768, September 2023. ISSN 1548-7105. doi: [10.1038/s41592-023-01969-x](https://doi.org/10.1038/s41592-023-01969-x). URL <http://dx.doi.org/10.1038/s41592-023-01969-x>.
- [42] Andrew Jaegle, Sebastian Borgeaud, Jean-Baptiste Alayrac, Carl Doersch, Catalin Ionescu, David Ding, Skanda Koppula, Daniel Zoran, Andrew Brock, Evan Shelhamer, et al. Perceiver IO: A General Architecture for Structured Inputs & Outputs. In *International Conference on Learning Representations*, 2022.
- [43] Andrew Jaegle, Felix Gimeno, Andy Brock, Oriol Vinyals, Andrew Zisserman, and Joao Carreira. Perceiver: General perception with iterative attention. In *International conference on machine learning*, pages 4651–4664. PMLR, 2021.

- [44] Anna Kuzina, Kumar Pratik, Fabio Valerio Massoli, and Arash Behboodi. Equivariant priors for compressed sensing with unknown orientation. In *International Conference on Machine Learning*, pages 11753–11771. PMLR, 2022.
- [45] Jakub Tomczak and Max Welling. Vae with a vampprior. In *International conference on artificial intelligence and statistics*, pages 1214–1223. PMLR, 2018.
- [46] Jonathan Ho and Tim Salimans. Classifier-free diffusion guidance. *arXiv preprint arXiv:2207.12598*, 2022.
- [47] Yaron Lipman, Ricky TQ Chen, Heli Ben-Hamu, Maximilian Nickel, and Matt Le. Flow matching for generative modeling. *arXiv preprint arXiv:2210.02747*, 2022.
- [48] Alexander Tong, Nikolay Malkin, Guillaume Hugué, Yanlei Zhang, Jarrid Rector-Brooks, Kilian Fatras, Guy Wolf, and Yoshua Bengio. Conditional flow matching: Simulation-free dynamic optimal transport. *arXiv preprint arXiv:2302.00482*, 2(3), 2023.
- [49] Irina Higgins, Loic Matthey, Arka Pal, Christopher Burgess, Xavier Glorot, Matthew Botvinick, Shakir Mohamed, and Alexander Lerchner. beta-VAE: Learning basic visual concepts with a constrained variational framework. In *International conference on learning representations*, 2017.
- [50] 10 Million Human PBMCs in a Single Experiment. <https://www.parsebiosciences.com/datasets/10-million-human-pbmcs-in-a-single-experiment/>. [Online; accessed on September 5, 2025].
- [51] Ajay Nadig, Joseph M Replogle, Angela N Pogson, Mukundh Murthy, Steven A McCarroll, Jonathan S Weissman, Elise B Robinson, and Luke J O’Connor. Transcriptome-wide analysis of differential expression in perturbation atlases. *Nature Genetics*, pages 1–10, 2025.
- [52] Haotian Cui, Chloe Wang, Hassaan Maan, Kuan Pang, Fengning Luo, Nan Duan, and Bo Wang. scGPT: toward building a foundation model for single-cell multi-omics using generative AI. *Nature methods*, 21(8):1470–1480, 2024.
- [53] Timothy Ting-Hsuan Wu, Kyle J Travaglini, Arjun Rustagi, Duo Xu, Yue Zhang, Leonid Andronov, SoRi Jang, Astrid Gillich, Roozbeh Dehghannasiri, Giovanni J Martínez-Colón, et al. Interstitial macrophages are a focus of viral takeover and inflammation in covid-19 initiation in human lung. *Journal of Experimental Medicine*, 221(6):e20232192, 2024.
- [54] The Tabula Sapiens Consortium and Stephen R Quake. Tabula sapiens reveals transcription factor expression, senescence effects, and sex-specific features in cell types from 28 human organs and tissues. *bioRxiv*, 2025. doi: 10.1101/2024.12.03.626516. URL <https://www.biorxiv.org/content/early/2025/08/27/2024.12.03.626516>.
- [55] James D Pearce, Sara E Simmonds, Gita Mahmoudabadi, Lakshmi Krishnan, Giovanni Palla, Ana-Maria Istrate, Alexander Tarashansky, Benjamin Nelson, Omar Valenzuela, Donghui Li, et al. A cross-species generative cell atlas across 1.5 billion years of evolution: The transcriptformer single-cell model. *bioRxiv*, pages 2025–04, 2025.
- [56] Nicholas Ho, Caleb N. Ellington, Jinyu Hou, Sohan Addagudi, Shentong Mo, Tianhua Tao, Dian Li, Yonghao Zhuang, Hongyi Wang, Xingyi Cheng, Le Song, and Eric P. Xing. Scaling dense representations for single cell with transcriptome-scale context. In *NeurIPS 2024 Workshop on AI for New Drug Modalities*. bioRxiv, 2024.
- [57] Christina V Theodoris, Ling Xiao, Anant Chopra, Mark D Chaffin, Zeina R Al Sayed, Matthew C Hill, Helene Mantineo, Elizabeth M Brydon, Zexian Zeng, X Shirley Liu, et al. Transfer learning enables predictions in network biology. *Nature*, 618(7965):616–624, 2023.
- [58] Yanay Rosen, Yusuf Roohani, Ayush Agarwal, Leon Samotorčan, Tabula Sapiens Consortium, Stephen R Quake, and Jure Leskovec. Universal cell embeddings: A foundation model for cell biology. *bioRxiv*, pages 2023–11, 2023.
- [59] Lily Zhang, Veronica Tozzo, John Higgins, and Rajesh Ranganath. Set norm and equivariant skip connections: Putting the deep in deep sets. In *International Conference on Machine Learning*, pages 26559–26574. PMLR, 2022.
- [60] Ashish Vaswani, Noam Shazeer, Niki Parmar, Jakob Uszkoreit, Llion Jones, Aidan N Gomez, Łukasz Kaiser, and Illia Polosukhin. Attention is all you need. *Advances in neural information processing systems*, 30, 2017.

- [61] Aaron Van Den Oord, Sander Dieleman, Heiga Zen, Karen Simonyan, Oriol Vinyals, Alex Graves, Nal Kalchbrenner, Andrew Senior, Koray Kavukcuoglu, et al. Wavenet: A generative model for raw audio. *arXiv preprint arXiv:1609.03499*, 12:1, 2016.
- [62] Jaeyeon Kim, Kulin Shah, Vasilis Kontonis, Sham M Kakade, and Sitan Chen. Train for the worst, plan for the best: Understanding token ordering in masked diffusions. In *Forty-second International Conference on Machine Learning*, 2025.
- [63] Arnaud Pannatier, Evann Courdier, and François Fleuret.  $\sigma$ -gpts: A new approach to autoregressive models. In *Joint European Conference on Machine Learning and Knowledge Discovery in Databases*, pages 143–159. Springer, 2024.
- [64] Jonathan Ho, Ajay Jain, and Pieter Abbeel. Denoising diffusion probabilistic models. *Advances in neural information processing systems*, 33:6840–6851, 2020.
- [65] Shen Nie, Fengqi Zhu, Chao Du, Tianyu Pang, Qian Liu, Guangtao Zeng, Min Lin, and Chongxuan Li. Scaling up masked diffusion models on text. In *The Thirteenth International Conference on Learning Representations*, 2025.
- [66] Arthur Gretton, Karsten M Borgwardt, Malte J Rasch, Bernhard Schölkopf, and Alexander Smola. A kernel two-sample test. *The journal of machine learning research*, 13(1):723–773, 2012.
- [67] L Theis, A van den Oord, and M Bethge. A note on the evaluation of generative models. In *International Conference on Learning Representations (ICLR 2016)*, pages 1–10, 2016.
- [68] Pau Badia-I-Mompel, Jesús Vélez Santiago, Jana Braunger, Celina Geiss, Daniel Dimitrov, Sophia Müller-Dott, Petr Taus, Aurelien Dugourd, Christian H Holland, Ricardo O Ramirez Flores, and Julio Saez-Rodriguez. decoupler: ensemble of computational methods to infer biological activities from omics data. *Bioinform. Adv.*, 2(1):vbac016, March 2022.

## A LLM Usage Disclaimer

We used large language models (ChatGPT and Claude) to assist with manuscript polishing, including grammar and clarity improvements, and to verify technical definitions and terminology. All scientific content, analysis, and conclusions are the original work of the authors.

## B Definitions

**Self-attention** Attention mechanism is defined as  $\text{Att}(\mathbf{Q}, \mathbf{K}, \mathbf{V}) \stackrel{df}{=} \text{softmax}(\mathbf{Q}\mathbf{K}^\top)\mathbf{V}$ , where  $\mathbf{Q} \in \mathbb{R}^{m \times D}$ ,  $\mathbf{K} \in \mathbb{R}^{M \times D}$ ,  $\mathbf{V} \in \mathbb{R}^{M \times D}$ , and  $\text{softmax}(\cdot)$  is the row-wise softmax function.<sup>4</sup> Typically,  $\mathbf{Q}$ ,  $\mathbf{K}$  and  $\mathbf{V}$  are results of linear transformations of given inputs. If all matrices are calculated based on the same input  $\mathbf{X}$ , we refer to it as *self-attention*.

**Cross-attention** However, if  $\mathbf{Q}$  is calculated using  $\mathbf{X}$ , and another input  $\mathbf{Y}$  is used to obtain  $\mathbf{K}$  and  $\mathbf{V}$ , then we refer to it as *cross-attention*.

**Multi-head attention**  $\text{Att}_K$  denotes a multi-head attention with  $K$  heads, i.e., a concatenation of  $K$  attention layers.

**Multi-head Attention Block (MAB)** A multi-head attention block (MAB) is defined as follows [31, 59]:

$$\begin{aligned} \text{MAB}(\mathbf{X}, \mathbf{Y}) &\stackrel{df}{=} f(\mathbf{X}, \mathbf{Y}) + \text{relu}(f(\mathbf{X}, \mathbf{Y})\mathbf{W}), \\ f(\mathbf{X}, \mathbf{Y}) &\stackrel{df}{=} \mathbf{X}\mathbf{W}_f + \text{Att}_K(\mathbf{Q}(\mathbf{X}), \mathbf{K}(\mathbf{Y}), \mathbf{V}(\mathbf{Y})), \end{aligned} \quad (9)$$

where  $f(\mathbf{X}, \mathbf{Y}) \stackrel{df}{=} \mathbf{X}\mathbf{W}_f + \text{Att}_K(\mathbf{Q}(\mathbf{X}), \mathbf{K}(\mathbf{Y}), \mathbf{V}(\mathbf{Y}))$ ,  $\mathbf{W}$  and  $\mathbf{W}_f$  are learnable weight matrices.

**Set Attention Block (SAB)** Set Attention Block (SAB) is defined as follows [31]:

$$\text{SAB}(\mathbf{X}) \stackrel{df}{=} \text{MAB}(\mathbf{X}, \mathbf{X}). \quad (10)$$

**Induced Set Attention Block (ISAB)** Induced Set Attention Block (ISAB) is defined as follows [31]:

$$\text{ISAB}(\mathbf{X}) \stackrel{df}{=} \text{MAB}(\mathbf{X}, \text{MAB}(\mathbf{U}, \mathbf{X})), \quad (11)$$

where  $\mathbf{U} \in \mathbb{R}^{m \times D}$  are *inducing points*, i.e., a global weight matrix learnable by backpropagation.

**Pooling by Multi-Head Attention** Pooling by Multi-head Attention (PMA) is defined as follows:

$$\text{PMA}(\mathbf{X}) = \text{MAB}(\mathbf{S}, \text{rFF}(\mathbf{X})), \quad (12)$$

where  $\mathbf{S} \in \mathbb{R}^{m \times D}$  is a matrix of learnable *inducing points* (or *pseudoinputs*), and  $\text{rFF} : \mathbb{R}^{M \times D} \rightarrow \mathbb{R}^{M \times D}$  is a row-wise linear layer. For fixed inducing points  $\mathbf{S}$  in PMA, this layer is permutation-invariant (this is due to applying the attention layer, see Property 3 in Appendix C).

<sup>4</sup>We skip scaling  $\mathbf{Q}\mathbf{K}^\top$  by  $1/\sqrt{D}$  to avoid unnecessary clutter.

## C Permutation-equivariance and Permutation-invariance of attention mechanism

The row-wise self-attention function fulfills the following property:

*Property 1.* For a given matrix  $\mathbf{X} \in \mathbb{R}^{M \times D}$ , and two permutation matrices  $\mathbf{P}_M \in \{0, 1\}^{M \times M}$  and  $\mathbf{P}_D \in \{0, 1\}^{D \times D}$ , the following statements hold true for the row-wise softmax function: (i)  $\text{softmax}(\mathbf{X}\mathbf{P}_D^\top) = \text{softmax}(\mathbf{X})\mathbf{P}_D^\top$ , (ii)  $\text{softmax}(\mathbf{P}_M\mathbf{X}) = \mathbf{P}_M\text{softmax}(\mathbf{X})$ .

Property 1 tells us that applying the permutation to the softmax function just reorders its columns/rows, hence, applying softmax before or after the reordering gives the same vector, merely shuffled.

Before we move to next properties, we recall that any permutation matrix is orthogonal, hence,  $\mathbf{P}\mathbf{P}^\top = \mathbf{P}^\top\mathbf{P} = \mathbf{I}$ .

It is a well-known fact that the (self-)attention mechanism is permutation-equivariant, namely, the following property holds true:

*Property 2.* For a given permutation matrix  $\mathbf{P} \in \{0, 1\}^{M \times M}$ , the attention mechanism is permutation-equivariant, i.e.,  $\text{Att}(\mathbf{P}\mathbf{Q}(\mathbf{X}), \mathbf{P}\mathbf{K}(\mathbf{X}), \mathbf{P}\mathbf{V}(\mathbf{X})) = \mathbf{P} \text{Att}(\mathbf{Q}(\mathbf{X}), \mathbf{K}(\mathbf{X}), \mathbf{V}(\mathbf{X}))$ .

*Proof.* First, we notice that:  $\mathbf{Q}(\mathbf{P}\mathbf{X}) = \mathbf{P}\mathbf{X}\mathbf{W}_Q = \mathbf{P}\mathbf{Q}(\mathbf{X})$ ,  $\mathbf{K}(\mathbf{P}\mathbf{X}) = \mathbf{P}\mathbf{X}\mathbf{W}_K = \mathbf{P}\mathbf{K}(\mathbf{X})$  and  $\mathbf{V}(\mathbf{P}\mathbf{X}) = \mathbf{P}\mathbf{X}\mathbf{W}_V = \mathbf{P}\mathbf{V}(\mathbf{X})$ . Next, to avoid unnecessary clutter, let us skip the dependency on  $\mathbf{X}$ . Then:

$$\begin{aligned} \text{Att}(\mathbf{P}\mathbf{Q}, \mathbf{P}\mathbf{K}, \mathbf{P}\mathbf{V}) &= \text{softmax}(\mathbf{P}\mathbf{Q}(\mathbf{P}\mathbf{K})^\top)\mathbf{P}\mathbf{V} \\ &= \text{softmax}(\mathbf{P}\mathbf{Q}\mathbf{K}^\top\mathbf{P}^\top)\mathbf{P}\mathbf{V} \\ &= \mathbf{P} \text{softmax}(\mathbf{Q}\mathbf{K}^\top)\mathbf{P}^\top\mathbf{P}\mathbf{V} \\ &= \mathbf{P} \text{softmax}(\mathbf{Q}\mathbf{K}^\top)\mathbf{V} \\ &= \mathbf{P} \text{Att}(\mathbf{Q}, \mathbf{K}, \mathbf{V}). \end{aligned}$$

□

The attention mechanism becomes permutation-invariant for  $\mathbf{Q}$  being a global parameter matrix only if the following property holds true:

*Property 3.* For a given permutation matrix  $\mathbf{P} \in \{0, 1\}^{M \times M}$ , the attention mechanism with inducing points  $\mathbf{Q} \in \mathbb{R}^{m \times D}$  is permutation-invariant, i.e.,  $\text{Att}(\mathbf{Q}, \mathbf{P}\mathbf{K}(\mathbf{X}), \mathbf{P}\mathbf{V}(\mathbf{X})) = \text{Att}(\mathbf{Q}, \mathbf{K}(\mathbf{X}), \mathbf{V}(\mathbf{X}))$ .

*Proof.* First, we notice that:  $\mathbf{K}(\mathbf{P}\mathbf{X}) = \mathbf{P}\mathbf{X}\mathbf{W}_K = \mathbf{P}\mathbf{K}(\mathbf{X})$  and  $\mathbf{V}(\mathbf{P}\mathbf{X}) = \mathbf{P}\mathbf{X}\mathbf{W}_V = \mathbf{P}\mathbf{V}(\mathbf{X})$ . Next, to avoid unnecessary clutter, let us skip the dependency on  $\mathbf{X}$ . Then:

$$\begin{aligned} \text{Att}(\mathbf{Q}, \mathbf{P}\mathbf{K}, \mathbf{P}\mathbf{V}) &= \text{softmax}(\mathbf{Q}(\mathbf{P}\mathbf{K})^\top)\mathbf{P}\mathbf{V} \\ &= \text{softmax}(\mathbf{Q}\mathbf{K}^\top\mathbf{P}^\top)\mathbf{P}\mathbf{V} \\ &= \text{softmax}(\mathbf{Q}\mathbf{K}^\top)\mathbf{P}^\top\mathbf{P}\mathbf{V} \\ &= \text{softmax}(\mathbf{Q}\mathbf{K}^\top)\mathbf{V} \\ &= \text{Att}(\mathbf{Q}, \mathbf{K}, \mathbf{V}). \end{aligned}$$

□

However, for a latent matrix  $\mathbf{Z} \in \mathbb{R}^{m \times D}$  obtained by transforming  $\mathbf{X}$  in the permutation-invariant manner, an embedding matrix  $\mathbf{E} \in \mathbb{R}^{V \times D}$ , the inducing points determined by a set of indices  $\mathcal{J}$ , i.e.,  $\mathbf{Q} = \mathbf{E}_{\mathcal{J}}$ , is permutation-equivariant if the indices  $\mathcal{J}$  are permuted, i.e., a permutation of indices  $\pi(\mathcal{J})$  induces the matrix  $\mathbf{P}$ , thus,  $\mathbf{P}\mathbf{Q} = \mathbf{E}_{\pi(\mathcal{J})}$ . Then, the following property holds true:

*Property 4.* For a given permutation of indices  $\mathcal{J}$ ,  $\pi(\mathcal{J})$ , or, equivalently, a matrix permutation  $\mathbf{P} \in \{0, 1\}^{|\mathcal{J}| \times |\mathcal{J}|}$ , and latents  $\mathbf{Z}$  calculated by a permutation-invariant function  $f$ , i.e.,  $\mathbf{Z} = f(\mathbf{P}\mathbf{X})$ , the attention mechanism with inducing points  $\mathbf{Q} \in \mathbb{R}^{|\mathcal{J}| \times D}$  is permutation-equivariant, i.e.,  $\text{Att}(\mathbf{P}\mathbf{Q}, \mathbf{K}(f(\mathbf{P}\mathbf{X})), \mathbf{V}(f(\mathbf{P}\mathbf{X}))) = \mathbf{P}\text{Att}(\mathbf{Q}, \mathbf{K}(\mathbf{Z}), \mathbf{V}(\mathbf{Z}))$ .

*Proof.* First, since  $f$  is permutation-invariance, we get  $\mathbf{Z} = f(\mathbf{PX}) = f(\mathbf{X})$ . Second, we note that  $\mathbf{K}(\mathbf{PZ}) = \mathbf{PZ}\mathbf{W}_K = \mathbf{PK}(\mathbf{Z})$  and  $\mathbf{V}(\mathbf{PZ}) = \mathbf{PZ}\mathbf{W}_V = \mathbf{PV}(\mathbf{Z})$ . Then:

$$\begin{aligned} \text{Att}(\mathbf{PQ}, \mathbf{K}(f(\mathbf{PX})), \mathbf{V}(f(\mathbf{PX}))) &= \text{softmax}(\mathbf{PQK}(f(\mathbf{PX}))^\top)\mathbf{V}(f(\mathbf{PX})) \\ &= \mathbf{P} \text{softmax}(\mathbf{QK}(f(\mathbf{X}))^\top)\mathbf{V}(f(\mathbf{X})) \\ &= \mathbf{P} \text{softmax}(\mathbf{QK}(\mathbf{Z})^\top)\mathbf{V}(\mathbf{Z}) \\ &= \mathbf{P} \text{Att}(\mathbf{Q}, \mathbf{K}(\mathbf{Z}), \mathbf{V}(\mathbf{Z})). \end{aligned}$$

□

## D Code

The implementation of our methods is available online at [<https://github.com/czi-ai/scLDM>]

## E Related Work (extended)

Modeling a probability distribution over order-agnostic objects like sets is challenging for at least two reasons. First, a model must be permutation-equivariant, meaning, changing the order of variables changes the order of parameters as well. Second, the model must also be exchangeable. Additionally, in the case of gene expression, for various tissues, we get different subsets of genes, thus, ideally, we would like to learn a single model to *transfer* hidden dependencies (correlations) among cells from distinct tissues.

**Autoregressive Models** A varying-size objects are typically modeled by autoregressive models (ARMs) like transformer-based LLMs for text [60] or WaveNet for audio [61]. However, ARMs assume a fixed order of variables, otherwise, like in the case of sets, their performance can drop significantly. Recently, it has been shown that misspecifying the order in ARMs can result in a huge drop in their performance [62]. There are ways of dealing with the order in ARMs [63], but they are not well-suited for processing objects without an explicitly defined order.

**Masked Diffusion Models** Recently, a masked version of diffusion-based models [64] are used to generate text quite successfully [65] since they can alleviate the need of specifying the order of generation. However, as proven in [62], masked diffusion-based models are order-agnostic but at the price of learning an extremely complex task of predicting a variable value conditioned on a set of unmasked variables in arbitrary positions.

**Variational Auto-Encoders** Another modeling approach is to define a Variational Auto-Encoder [23, 24] since this framework allows defining its components in a flexible manner. In [25], a SetVAE was formulated by introducing two separate latent variables to deal with varying size of sets, namely,  $\mathbf{z}_J$  of the same dimensionality as  $\mathbf{x}_J$  such that  $\mathbf{z}_i$  corresponds to  $\mathbf{x}_i$ ,  $i \in J$ , and an additional vector of latents  $\mathbf{c} \in \mathbb{R}^{d_1}$  of a constant size  $d_1$ . In general,  $\mathbf{x}_J$  can be generated given  $\mathbf{z}_J$  and each  $\mathbf{z}_i$  is generated given  $\mathbf{c}$ , i.e.,  $p(\mathbf{x}_J|J, \mathbf{z}_J) p(\mathbf{z}_J|\mathbf{c}) p(\mathbf{c})$ , where  $p(\mathbf{x}_J|J, \mathbf{z}_J) = \prod_{i=1}^{|J|} p(\mathbf{x}_i|\mathbf{z}_i)$  and  $p(\mathbf{z}_J|\mathbf{c}) = p(|J|) \prod_{i=1}^{|J|} p(\mathbf{z}_i|\mathbf{c})$ . Then, the variational posteriors can take the following form:  $q(\mathbf{z}_J|\mathbf{x}_J) = \delta(|J|) \prod_{i=1}^{|J|} q(\mathbf{z}_i|\mathbf{x}_i)$ , where  $\delta(\cdot)$  is Dirac's delta, and additionally we have  $q(\mathbf{c}|\mathbf{x}_J)$ . In [25], a few simplifications were made such that the model fits well modeling point clouds (sets of 3-D points), namely, for all  $i = 1, \dots, |J|$ ,  $p(\mathbf{z}_i|\mathbf{c}) = p(\mathbf{z}_i)$ , and  $q(\mathbf{z}_i|\mathbf{c}) = p(\mathbf{z}_i)$ . Further, the authors of [25] suggested to define a hierarchical VAE with multiple layers of  $\mathbf{z}_J$ 's and  $\mathbf{c}$ 's since a single layer did not result in good performance, and they replaced the conditional likelihood with Chamfer Distance as a well-suited distance for point clouds. In this paper, we find a great appeal of the VAE framework and its flexibility; however, we claim using two distinct latents and a hierarchical latent structure to be unnecessary. Instead, we suggest picking a careful parameterization to be *crucial* in obtaining high performance.

**Permutation-equivariant/invariant Parameterizations** Deep Neural Networks are widely used as transformations of raw data and parameterizations of probability distributions. It is advocated (but also observed empirically) that modeling probability distributions requires utilizing symmetries in data [26]. For instance, for objects whose dimensions can be shuffled without changing the underlying latent structure, we need either *permutation-invariant* or *permutation-equivariant* transformations. For a given permutation matrix  $\mathbf{P}$ , a function  $f : \mathbb{X} \rightarrow \mathbb{Y}$  is *permutation-invariant* if  $f(\mathbf{P}\mathbf{x}) = \mathbf{y}$ ; on the other hand, a function  $f : \mathbb{X} \rightarrow \mathbb{Y}$  is *permutation-equivariant* if  $f(\mathbf{P}\mathbf{x}) = \mathbf{P}\mathbf{y}$ .

A general *blueprint* for composing geometric deep neural networks is a composition of permutation-invariant layers and/pr permutation-equivariant layers, with nonlinearity activation functions in between [26]. An example of such a blueprint is an architecture called DeepSets [27]. It formulates a general permutation-equivariance layer treating all variables consistently regardless their positions. Then it applies a symmetric aggregation like averaging or other pooling operators [28–30] to combine these equivariant features in a permutation-invariant fashion, ensuring the order of inputs does not affect the output. The drawback of this approach is that all elements are processed separately before being aggregated with a non-learnable pooling operator. This manner of constructing permutation-invariant transformations might be highly limiting.

A potential solution to that issue is replacing static pooling with a learned attention mechanism, allowing utilizing transformer-based architectures to transform all elements jointly in an equivariant and invariant fashion. An example of a fully-transformer-based model is SetTransformer [31] that builds on the following idea. Attention mechanism is defined as  $\text{Att}(\mathbf{Q}, \mathbf{K}, \mathbf{V}) \stackrel{df}{=} \text{softmax}(\mathbf{Q}\mathbf{K}^\top)\mathbf{V}$ , where  $\mathbf{Q} \in \mathbb{R}^{m \times D}$ ,  $\mathbf{K} \in \mathbb{R}^{M \times D}$ ,  $\mathbf{V} \in \mathbb{R}^{M \times D}$ , and  $\text{softmax}(\cdot)$  is the row-wise softmax function.<sup>5</sup> Typically,  $\mathbf{Q}$ ,  $\mathbf{K}$  and  $\mathbf{V}$  are results of linear transformations of some inputs. If all matrices are calculated based on the same input  $\mathbf{X}$ , we refer to it as *self-attention*. However, if  $\mathbf{Q}$  is calculated using  $\mathbf{X}$ , and another input  $\mathbf{Y}$  is used to obtain  $\mathbf{K}$  and  $\mathbf{V}$ , then we refer to it as *cross-attention*. Let  $\text{Att}_K$  denote a multi-head attention with  $K$  heads, i.e., a concatenation of  $K$  attention layers. SetTransformer introduces a multi-head attention block (MAB) [31, 59]:

$$\begin{aligned} \text{MAB}(\mathbf{X}, \mathbf{Y}) &\stackrel{df}{=} f(\mathbf{X}, \mathbf{Y}) + \text{relu}(f(\mathbf{X}, \mathbf{Y})\mathbf{W}), \\ f(\mathbf{X}, \mathbf{Y}) &\stackrel{df}{=} \mathbf{X}\mathbf{W}_f + \text{Att}_K(\mathbf{Q}(\mathbf{X}), \mathbf{K}(\mathbf{Y}), \mathbf{V}(\mathbf{Y})), \end{aligned} \quad (13)$$

where  $f(\mathbf{X}, \mathbf{Y}) \stackrel{df}{=} \mathbf{X}\mathbf{W}_f + \text{Att}_K(\mathbf{Q}(\mathbf{X}), \mathbf{K}(\mathbf{Y}), \mathbf{V}(\mathbf{Y}))$ ,  $\mathbf{W}$  and  $\mathbf{W}_f$  are learnable weight matrices. Given MAB, SetTransformer further defines the following two blocks, namely, the Set Attention Block (SAB) and Induced Set Attention Block (ISAB):  $\text{SAB}(\mathbf{X}) \stackrel{df}{=} \text{MAB}(\mathbf{X}, \mathbf{X})$ , and  $\text{ISAB}(\mathbf{X}) \stackrel{df}{=} \text{MAB}(\mathbf{X}, \text{MAB}(\mathbf{U}, \mathbf{X}))$ , where  $\mathbf{U} \in \mathbb{R}^{m \times D}$  are *inducing points*, i.e., a global weight matrix learnable by backpropagation. ISAB allows to change the size of the input, and similarly to SAB, it is permutation-equivariant [31]. To obtain a permutation-invariant transformation, SetTransformer proposes to use another layer called Pooling by Multi-head Attention (PMA):

$$\text{PMA}(\mathbf{X}) = \text{MAB}(\mathbf{S}, \text{rFF}(\mathbf{X})), \quad (14)$$

where  $\mathbf{S} \in \mathbb{R}^{m \times D}$  is a matrix of learnable *inducing points* (or *pseudoinputs*), and  $\text{rFF} : \mathbb{R}^{M \times D} \rightarrow \mathbb{R}^{M \times D}$  is a row-wise linear layer. For fixed inducing points  $\mathbf{S}$  in PMA, this layer is permutation-invariant (this is due to applying the attention layer, see Property 3 in Appendix C). These building blocks can be used to formulate a deep neural network for parameterizing a probabilistic model. However, we advocate for a different parameterization that applies a single multi-head attention layer in a transformer block to obtain a fixed-size output, and then a series of transformer blocks.

**Latent Diffusion Models** Latent Diffusion Models (LDMs) perform diffusion processes in learned latent spaces rather than directly in high-dimensional data spaces. Stable Diffusion [32] pioneered this approach for text-to-image synthesis by training diffusion models in the latent space of a pre-trained VAE, dramatically reducing computational costs while maintaining generation quality. This paradigm has proven effective across diverse scientific domains: all-atom diffusion transformers [33] generate molecules

<sup>5</sup>We skip scaling  $\mathbf{Q}\mathbf{K}^\top$  by  $1/\sqrt{D}$  to avoid unnecessary clutter.

and materials with atomic-level precision, similiary LaM-SLidE [34] utilizes transformer-based LMD for molecular dynamics (among others), while La-proteina [35] employs transformer-based partially latent flow matching for atomistic protein generation. These advances demonstrate the versatility of latent diffusion approaches for complex, high-dimensional scientific data across multiple modalities. Here, we extend this framework to single-cell transcriptomics by proposing a transformer-based LDM for this biological data type.

**Generative Models for scRNA-seq** In the context of single-cell genomics, numerous generative models have been developed for (conditional) sampling of gene expression profiles. scVI [12] represents an early VAE-based generative model, while more recent approaches include GAN-based and diffusion-based architectures such as scGAN [36] and scDiffusion [19]. These models operate in continuous space and therefore transform discrete gene expression data into log-normalized counts. Recently, latent diffusion frameworks have emerged with models like SCLD [37] and CFGen [20], which leverage latent diffusion frameworks. Additionally, application-specific generative models have been developed for perturbational single-cell genomics, including CPA [38], SquiDiff [39], CellFlow [40], and CellOT [41], which are tailored to capture the effects of genetic and chemical perturbations on cellular states. Our approach is similar in vein to CFGen and SCLD, but leverages transformer-based architectures for both our newly proposed VAE as well as the latent diffusion model.

## F Our Approach: Additional information

### F.1 Gene expression data embedding: Replacing *dropouts*

We present a method for processing sparse gene expression data that focuses computational resources on biologically relevant signals. Given a set of  $D$  genes with their corresponding expression counts, our approach addresses the inherent sparsity in single-cell RNA sequencing data, where typically 70% or more of gene-cell entries are zero.

Let  $\mathcal{J} = \{1, 2, \dots, D\}$  denote the complete set of gene IDs represented as integers, and let  $\mathbf{x} = (x_1, x_2, \dots, x_D)$  represent the corresponding gene expression counts for a given cell, where  $x_i \in \mathbb{N}_0$  is the count for gene  $g_i$ , then an  $n$ -th single cell is defined as a tuple  $(\mathbf{x}_{\mathcal{J}_n}, \mathcal{J}_n)$ .

Our method proceeds as follows:

- (1) **Context length constraint:** We define a maximum context length  $d < D$  to limit the computational complexity of downstream processing.
- (2) **Expression-based filtering:** For each cell, we identify the set of expressed genes:

$$\mathcal{E} = \{i \in \mathcal{J} : x_i > 0\} \quad (15)$$

with corresponding expression values  $\mathbf{x}_{\mathcal{E}} = \{x_i : i \in \mathcal{E}\}$ .

- (3) **Context construction:** We construct a fixed-length input representation of dimension  $d$ . When  $|\mathcal{E}| < d$  (which is typically the case due to high sparsity), we pad the input with artificial tokens to maintain consistent dimensionality:

$$\text{Input} = \begin{cases} \{(x_i, i)\}_{i \in \mathcal{E}} \cup \{(0, \text{PAD})\}^{d-|\mathcal{E}|} & \text{if } |\mathcal{E}| < d \\ \{(x_i, i)\}_{i \in \mathcal{E}} & \text{if } |\mathcal{E}| = d \end{cases} \quad (16)$$

where PAD is a special token for zero expression count.

This approach offers both computational and biological advantages. By excluding zero-expression genes (dropouts) from the input representation, we enable the model to focus exclusively on expressed genes, which carry the meaningful biological signal. The padding tokens serve purely as placeholders for implementation consistency and do not introduce spurious biological information, as they are explicitly marked with zero counts. This design choice aligns with the biological understanding that in single-cell data, the absence of detected expression often represents technical dropouts rather than meaningful biological zeros, making it advantageous to direct the model’s attention solely to the detected expression events.

## F.2 Conditional likelihood: The parameterization of Negative Binomial

We model the gene expression counts using a Negative Binomial distribution, which effectively captures the overdispersion commonly observed in single-cell RNA-seq data. The conditional likelihood for our model is specified as follows.

Let  $\mathbf{h}(\mathbf{Z}) \in \mathbb{R}^D$  denote the output of our neural network for a given cell embedding  $\mathbf{Z}$ , where  $D$  is the number of genes. We apply a softmax transformation to obtain normalized ratios:

$$p_i(\mathbf{Z}) = \frac{\exp(\mathbf{h}_i(\mathbf{Z}))}{\sum_{j=1}^D \exp(\mathbf{h}_j(\mathbf{Z}))} \quad (17)$$

where  $i = 1, 2, \dots, D$ , and  $\sum_{i=1}^D p_i = 1$ .

To obtain the expected expression counts, we scale these probabilities by the cell-specific library size  $L$ , namely:

$$\eta_i(\mathbf{Z}) = L \cdot p_i(\mathbf{Z}) \quad (18)$$

where  $\mu_i$  represents the mean parameter for gene  $i$  in the Negative Binomial distribution.

The gene expression count  $x_i$  for gene  $i$  is then modeled as:

$$x_i \sim \text{NB}(\eta_i(\mathbf{Z}), \alpha_i) \quad (19)$$

where NB denotes the Negative Binomial distribution parameterized by mean  $\mu_i$  and dispersion  $\alpha_i$ . The probability mass function is given by:

$$p(x_i | \eta_i(\mathbf{Z}), \alpha_i) = \frac{\Gamma(x_i + \alpha_i^{-1})}{\Gamma(x_i + 1)\Gamma(\alpha_i^{-1})} \left( \frac{\alpha_i^{-1}}{\alpha_i^{-1} + \eta_i(\mathbf{Z})} \right)^{\alpha_i^{-1}} \left( \frac{\eta_i(\mathbf{Z})}{\alpha_i^{-1} + \eta_i(\mathbf{Z})} \right)^{x_i} \quad (20)$$

We consider two parameterizations for the dispersion:

- (1) **Shared dispersion:** A single parameter  $\alpha$  is used for all genes, i.e.,  $\alpha_i = \alpha$  for all  $i \in \{1, 2, \dots, D\}$ . This reduces the number of parameters and assumes homogeneous overdispersion across genes.
- (2) **Gene-specific dispersion:** Each gene has its own dispersion parameter, resulting in a vector  $\boldsymbol{\alpha} = (\alpha_1, \alpha_2, \dots, \alpha_D)$ . This allows for heterogeneous overdispersion patterns across genes, providing greater flexibility at the cost of additional parameters.

This formulation ensures that the predicted expression values respect the constraint that total counts sum to the observed library size, while the Negative Binomial distribution appropriately models the count nature and overdispersion of the data. The softmax transformation guarantees that the neural network learns a proper distribution over genes, making the model interpretable as learning the relative expression probabilities for each cell.

## G Datasets

**General** In our experiments, we used the following datasets: Dentate gyrus, Tabula Muris, Human Lung Census Atlas (HLCA), Parse1M and Replogle-Nadig; see Table 6 for details.

**Experiment 1: Cell generation (benchmarks)** In the cell generation experiment, we used three widely used datasets, namely, Dentate gyrus, Tabula Muris, and HLCA. Dentate gyrus is the smallest dataset (only 18k cell and 17k genes). Tabula Muris is a small dataset with over 245k cells and almost 20k genes. Human Lung Cell Atlas (HLCA) is the largest, having about 585k cells and almost 28k genes.

**Experiment 2: Parse1M & Replogle** In the second experiment, we used a curated subset of 10 Million Human PBMC dataset. We carried out experiments on 2k highly variable genes (HVGs). In this data, we focused on a single donor who had 18 cell types undergone 90 cytokine perturbations as well as a control treatment. We left out for testing the cell type 'CD4 Naive' and 27 cytokine perturbations.

Next, we used the well-known Replogle-Nadig dataset which consists of four cell lines and 2024 gene-edits. We carried out experiments on 2k highly variable genes (HVGs). All 2024 gene-edits in three cell-lines ('jurkat', 'k562', 'rpe1'), along with a subset of edits from the 'hepg2' cell line were used for training. The remaining 'hepg2' gene-edits were held out for testing. We held out 372 gene edits from hepg2 cells.

**Experiment 3: COVID-19 and Tabula Sapiens 2.0** In the fourth experiment, we used two datasets for embedding evaluation. First, we used the scRNA-seq experimental dataset of four healthy donors' lung sections infected with SARS-CoV-2 [53]. Data were downloaded from CZ CELLxGENE<sup>6</sup>. Second, we used the Tabula Sapiens 2.0 dataset [54], a comprehensive single-cell atlas of human tissues. We focused on 6 tissues: blood, spleen, lymph node, small intestine, thymus, and liver. We filtered out cell types with fewer than 100 cells to ensure robust classification performance and used the resulting filtered dataset for multinomial logistic regression-based cell type prediction tasks.

TABLE 6. Summary of datasets used in the experiments.

Experiment	Dataset name	No. of cells	No. of genes	No. of cell types/lines
1	Dentate gyrus	18,213	17,002	14 cell types
1	Tabula Muris	245,389	19,734	123 cell types
1	HLCA	584,944	27,997	50 cell types
2	Parse1M	1,267,690	2,000 (HVGs)	18 cell types
2	Replogle-Nadig	624,158	2,000 (HVGs)	4 cell lines
3	COVID-19	354,026	27,998	55 cell types
3	Tabula Sapiens 2.0	1,482,026	~ 25k	22 cell types

## H Baselines

**scVI** Single-cell Variational Inference (scVI) [12] is VAE-based generative models designed for single-cell discrete data. Following the standard VAE framework, this model learns a Gaussian latent space that is subsequently decoded into the parameters of a discrete conditional likelihood model. For the reconstruction. For the observational data experiments, we implemented our own scVI model following default parameters from [20]. For the perturbational dataset, we used the implementation from the State [5] reproducibility repo <https://github.com/ArcInstitute/State-reproduce>, using default parameters. We train the models for 120k steps.

**scDiffusion** A version of a latent diffusion model for single-cell gene expression data is scDiffusion [19]. The scDiffusion model consists of three modules. The first module is an auto-encoder that transforms gene expression patterns into a compact representation space, allowing dimensionality reduction and identification of complex cellular measurements. In the latent space, a denoising network is trained to reverse a diffusion process applied to the latent embeddings, turning noise into meaningful biological signal encoded in the latent space. To ensure guided generation, a third model is trained, a classifier, for incorporating cell type or other biological attributes.

**CFGen** CFGen is a current state-of-the-art latent diffusion model that builds upon scVI, training a latent flow matching model in the VAE's latent space [20]. Similar to our approach, CFGen employs a two-stage training strategy: first training the autoencoder, then training the flow matching model on the VAE-generated embeddings. While CFGen introduces additive steering through classifier-free guidance, we utilize joint attribute control (see Table 15). However, since in the observational experiments we only conditioned on a single attribute, we do not think this is the source of the performance difference. Additionally, CFGen

<sup>6</sup><https://cellxgene.cziscience.com/collections/2a9a17c9-1f61-4877-b384-b8cd5ffa4085>

models the library size within the diffusion framework and samples from the mean and standard deviation of the library size distribution for conditional generation. We adapted this approach for sampling library size in our Negative Binomial conditional likelihood; however, unlike CFGen, we do not condition our Diffusion Transformer model on library size. We did not retrain CFGen but used the checkpoints for each observational dataset from the original repository. We followed the notebook for sampling from the model using guidance value of 1 (default).

**CPA** Compositional Perturbation Autoencoder (CPA) [13] is a deep generative model developed to predict gene expression changes under perturbations and their combinations. CPA disentangles latent representations of basal cellular state, perturbation effects, and additional covariates such as cell type. By recombining these factors through its decoder, CPA can reconstruct observed expression profiles and generalize to unseen perturbation–covariate combinations. This compositional structure enables CPA to extrapolate beyond training data, making it particularly well-suited for evaluating out-of-distribution generalization in perturbational single-cell datasets. For each dataset (Replogle and Parse1M) we trained 3 models with different seeds, but the same leave-out test set. We used the implementation from the State [5] reproducibility repo <https://github.com/ArcInstitute/State-reproduce>, using default parameters. We train the models for 120k steps.

**scGPT** For each dataset (Replogle and Parse1M) we trained 3 models with different seeds, but the same leave-out test set. We used as baseline the scGPT [52] model in the ‘genetic’ configuration for the Replogle-Nadig dataset, and in the ‘chemical’ configuration for the Parse 1M dataset. We used the implementation from the State [5] reproducibility repo <https://github.com/ArcInstitute/State-reproduce>, using default parameters. We train both scGPT models for 80k steps. For the ‘genetic’ configuration, we noticed that not all genes were present in the vocabulary (scGPT human downloaded from the original repo, following the baseline reproducibility repo from STATE), and that some genetic perturbations would be dropped. Hence, we built a feature set that consists of the union of 2000 HVG as well as the 2024 genetic perturbations, recovering 3482 genes. The ‘scGPT genetic’ model was therefore trained on 3482 genes, but evaluated on 1962 genes, which correspond to the subset of HVG that are part of the scGPT vocabulary. For the ‘chemical’ configuration, we trained on the same feature set of the rest of the baselines 2000 HVG.

**STATE** For each dataset (Replogle and Parse1M) we trained 3 models with different seeds, but the same leave-out test set. We used the STATE-Tx implementation from <https://github.com/ArcInstitute/State-reproduce> and trained for 80k steps for both datasets. We used the model configurations used in this notebook [https://colab.research.google.com/drive/1Ih-KtTESPqDQnjTh6etVv\\_f-gRAA86ZN](https://colab.research.google.com/drive/1Ih-KtTESPqDQnjTh6etVv_f-gRAA86ZN) for both datasets.

**Perturb mean** The Perturbation Mean baseline provides predictions by combining cell-type-specific control means with learned perturbation effects. The model operates as follows:

For each cell type  $c$  and perturbation  $p$ , we calculate separate means for control and perturbed populations:

$$\mu_c^{\text{ctrl}} = \frac{1}{|\mathcal{C}_c|} \sum_{i \in \mathcal{C}_c} \mathbf{x}^{(i)}, \quad \mu_{c,p}^{\text{pert}} = \frac{1}{|\mathcal{P}_{c,p}|} \sum_{i \in \mathcal{P}_{c,p}} \mathbf{x}^{(i)} \quad (21)$$

Here,  $\mathcal{C}_c$  denotes the collection of control (ctrl) cells belonging to type  $c$ , while  $\mathcal{P}_{c,p}$  represents perturbed cells of type  $c$  that received perturbation  $p$ . The cell-type-specific perturbation effect is computed as:

$$\delta_{c,p} = \mu_{c,p}^{\text{pert}} - \mu_c^{\text{ctrl}} \quad (22)$$

To obtain a global perturbation effect, we average these cell-type-specific effects across all cell types where the perturbation was applied:

$$\delta_p = \frac{1}{|\mathcal{C}_p|} \sum_{c \in \mathcal{C}_p} \delta_{c,p}, \quad \text{where } \mathcal{C}_p = \{c \mid |\mathcal{P}_{c,p}| > 0\} \quad (23)$$

For prediction, given a test cell of type  $t$  and perturbation  $p$ , the model generates:

$$\hat{\mathbf{x}} = \boldsymbol{\mu}_t^{\text{ctrl}} + \boldsymbol{\delta}_p, \quad \boldsymbol{\delta}_{\text{ctrl}} = \mathbf{0} \quad (24)$$

This approach ensures that control cells are predicted without modification, while perturbed cells receive a consistent global perturbation shift regardless of their specific cell type.

**Hepg2 and CD4 mean, context mean** The Context Mean baseline predicts a cell’s post-perturbation profile by returning the average perturbed expression of cells of the same cell type observed in the training set. For every cell type  $c$ , we collect all training cells whose perturbation is not the control and form the pseudo-bulk mean:

$$\boldsymbol{\mu}_c = \frac{1}{|\mathcal{J}_c|} \sum_{i \in \mathcal{J}_c} \mathbf{x}^{(i)}, \quad \mathcal{J}_c = \{i \mid \text{cell\_type}(i) = c, p^{(i)} \neq \text{ctrl}\}. \quad (25)$$

At inference time, for a test cell  $i$  with cell type  $c^{(i)}$  and perturbation label  $p^{(i)}$ , we predict:

$$\hat{\mathbf{x}}^{(i)} = \begin{cases} \mathbf{x}^{(i)} & \text{if } p^{(i)} = \text{ctrl}, \\ \boldsymbol{\mu}_{c^{(i)}} & \text{if } p^{(i)} \neq \text{ctrl}. \end{cases} \quad (26)$$

In other words, control cells are passed through unchanged, whereas perturbed cells inherit their cell-type mean.

## I Implementation details

In this paper, we carried out model selection for various values of hyperparameters. In the following paragraphs, we provide further details for reproducibility.

**VAE** Table 7 summarizes the hyperparameter configurations used for the VAE encoder architectures in our experiments.

TABLE 7. Hyperparameter values of VAE Encoders considered in this paper.

<b>VAE Encoder</b>	
<b>Embedding layer</b>	
Embedding size	256
<b>Cross-Attention Block</b>	
Number of Heads	{1,4,8}
No. pseudoinputs	{64,128, 256}
Embedding size	{128,256}
<b>Transformer Blocks</b>	
Number of Blocks	{2, 4}
Number of Heads	1
Embedding size	256
<b>Gaussian Stochastic Layer</b>	
Latents per token	{8, 16, 32}

Table 8 summarizes the hyperparameter configurations used for the VAE decoder architectures in our experiments.

TABLE 8. Hyperparameter values of VAE Decoders considered in this paper.

<b>VAE Decoder</b>	
<b>Transformer Blocks</b>	
Number of Blocks	{2, 4}
Number of Heads	{1,4,8}
Embedding size	{128,256}
Normalization	LayerNorm
<b>Cross-Attention Block</b>	
Shared embedding layer	True
No. pseudoinputs	{64,128, 256}
Number of Heads	1
Embedding size	256
<b>Negative Binomial Stochastic Layer</b>	
Shared $\theta$	False

**Flow Matching** Table 9 summarizes the hyperparameter configurations used for the LDM architectures in our experiments.

TABLE 9. Hyperparameter values of LDMs considered in this paper.

<b>LDM – Flow Matching</b>	
<b>Denosing Transformer</b>	
Number of Blocks	8
Number of Heads	8
Embedding size	256
Normalization	LayerNorm
Adaptive Normalization	True
<b>Hyperparams</b>	
$\sigma$	$1e^{-4}$
$\nu$	0
Transport	linear

**scLDM-VAE Census** Table 10 summarizes the hyperparameter configurations used for the scLDM-VAE Census architectures in our experiments.

**Training details** For training, we swept over various configurations of hyperparameters, see Table 11.

TABLE 10. Hyperparameter values of scLDM-VAE Census.

<b>Encoder-Decoder hyperparameters</b>	
Number of Blocks	{8,16}
Number of Heads	{8,16}
Number of Layers	{8,16}
Number of Latent Tokens	{256}
Embedding size	{256,512,768}
Normalization	LayerNorm

TABLE 11. Hyperparameter values of training procedures considered in this paper.

<b>Training</b>	
KL-weight	{0, 1e <sup>-5</sup> }
Optimizer	AdamW
Mini-batch size	{64,128,256}
Learning rate	{1e <sup>-3</sup> , 5e <sup>-4</sup> }
( $\beta_1, \beta_2$ )	(0.9, 0.95)
Weight Decay	{0, 1e <sup>-7</sup> , 1e <sup>-4</sup> }
Learning scheduler	cosine

## J Evaluation

### J.1 Maximum Mean Discrepancy (MMD)

We propose to use the Maximum Mean Discrepancy (MMD) [66]. MMD is a non-parametric distance measure between probability distributions based on the notion of embedding distributions into a reproducing kernel Hilbert space (RKHS)  $\mathcal{H}$ . Given two distributions  $P$  and  $Q$  over a domain  $\mathcal{X}$ , the MMD is defined as:

$$\text{MMD}[\mathcal{F}, P, Q] = \sup_{f \in \mathcal{F}} (\mathbb{E}_{x \sim P}[f(x)] - \mathbb{E}_{y \sim Q}[f(y)]), \quad (27)$$

where  $\mathcal{F}$  is a class of functions. When  $\mathcal{F}$  is the unit ball in an RKHS  $\mathcal{H}$  with kernel  $k$ , the MMD can be expressed as:

$$\text{MMD}^2[\mathcal{H}, P, Q] = \mathbb{E}_{x, x' \sim P}[k(x, x')] + \mathbb{E}_{y, y' \sim Q}[k(y, y')] - 2\mathbb{E}_{x \sim P, y \sim Q}[k(x, y)]. \quad (28)$$

In practice, given finite samples  $X = \{x_1, \dots, x_m\}$  drawn from  $P$  and  $Y = \{y_1, \dots, y_n\}$  drawn from  $Q$ , we use the unbiased empirical estimate:

$$\widehat{\text{MMD}}^2[X, Y] = \frac{1}{m(m-1)} \sum_{i \neq j}^m k(x_i, x_j) + \frac{1}{n(n-1)} \sum_{i \neq j}^n k(y_i, y_j) - \frac{2}{mn} \sum_{i=1}^m \sum_{j=1}^n k(x_i, y_j). \quad (29)$$

The choice of kernel  $k$  determines the richness of the function class  $\mathcal{F}$ . Common choices include the Gaussian RBF kernel  $k(x, y) = \exp(-\|x - y\|^2/2\sigma^2)$  with bandwidth parameter  $\sigma$ . The MMD is zero if and only if  $P = Q$  when using a characteristic kernel, making it a powerful tool for two-sample testing and distribution matching applications.

## J.2 2-Wasserstein Distance (W2)

The 2-Wasserstein distance provides an alternative metric for comparing probability distributions based on optimal transport theory. For distributions  $P$  and  $Q$  on  $\mathbb{R}^d$ , the 2-Wasserstein distance is defined as:

$$W_2(P, Q) = \left( \inf_{\gamma \in \Gamma(P, Q)} \int_{\mathbb{R}^d \times \mathbb{R}^d} \|\mathbf{x} - \mathbf{y}\|^2 d\gamma(\mathbf{x}, \mathbf{y}) \right)^{1/2}, \quad (30)$$

where  $\Gamma(P, Q)$  denotes the set of all joint distributions with marginals  $P$  and  $Q$ . For empirical distributions with equal sample sizes  $n$ , given samples  $X = \{\mathbf{x}_1, \dots, \mathbf{x}_n\}$  and  $Y = \{\mathbf{y}_1, \dots, \mathbf{y}_n\}$ , the discrete 2-Wasserstein distance simplifies to:

$$W_2^2(X, Y) = \frac{1}{n} \min_{\pi \in \Pi_n} \sum_{i=1}^n \|\mathbf{x}_i - \mathbf{y}_{\pi(i)}\|^2, \quad (31)$$

where  $\Pi_n$  is the set of all permutations of  $\{1, \dots, n\}$ . This optimization problem can be solved efficiently using the Hungarian algorithm or entropic regularization approaches.

When both distributions are Gaussian with means  $\boldsymbol{\mu}_P, \boldsymbol{\mu}_Q$  and covariances  $\boldsymbol{\Sigma}_P, \boldsymbol{\Sigma}_Q$ , the 2-Wasserstein distance has a closed-form expression:

$$W_2^2(P, Q) = \|\boldsymbol{\mu}_P - \boldsymbol{\mu}_Q\|^2 + \text{tr} \left( \boldsymbol{\Sigma}_P + \boldsymbol{\Sigma}_Q - 2(\boldsymbol{\Sigma}_P^{1/2} \boldsymbol{\Sigma}_Q \boldsymbol{\Sigma}_P^{1/2})^{1/2} \right), \quad (32)$$

which coincides with the Fréchet Distance.

Unlike MMD, the Wasserstein distance directly captures the geometry of the underlying space and provides interpretable transport plans between distributions.

## J.3 Fréchet Distance for Gene Expression Profile Evaluation

We adapt the Fréchet Inception Distance (FID) framework to evaluate the quality of synthetic gene expression profiles by replacing the Inception network's feature extraction with Principal Component Analysis (PCA). This approach provides a computationally efficient and interpretable metric for comparing distributions of real and synthetic gene expression data.

### J.3.1 Principal Components Calculation

Let  $\mathcal{X}_r = \{\mathbf{x}_1^r, \mathbf{x}_2^r, \dots, \mathbf{x}_n^r\}$  denote the set of real gene expression profiles and  $\mathcal{X}_s = \{\mathbf{x}_1^s, \mathbf{x}_2^s, \dots, \mathbf{x}_m^s\}$  denote the synthetic profiles, where each  $\mathbf{x}_i \in \mathbb{R}^D$  represents the expression levels of  $D$  genes.

We first apply PCA to the combined dataset to obtain a projection matrix  $\mathbf{W} \in \mathbb{R}^{k \times D}$  containing the top  $k$  principal components (e.g.,  $k = 30$ ). The feature representations are computed as:

$$\mathbf{z}_i^r = \mathbf{W}^\top \mathbf{x}_i^r, \quad \mathbf{z}_j^s = \mathbf{W}^\top \mathbf{x}_j^s \quad (33)$$

where  $\mathbf{z}_i^r, \mathbf{z}_j^s \in \mathbb{R}^k$  are the projected representations in the principal component space.

### J.3.2 Fréchet Distance Calculation

Assuming the feature representations follow multivariate Gaussian distributions:

- Real data:  $\mathcal{N}(\boldsymbol{\mu}_r, \boldsymbol{\Sigma}_r)$ ;
- Synthetic data:  $\mathcal{N}(\boldsymbol{\mu}_s, \boldsymbol{\Sigma}_s)$ .

We estimate the parameters:

$$\boldsymbol{\mu}_r = \frac{1}{n} \sum_{i=1}^n \mathbf{z}_i^r, \quad \boldsymbol{\Sigma}_r = \frac{1}{n-1} \sum_{i=1}^n (\mathbf{z}_i^r - \boldsymbol{\mu}_r)(\mathbf{z}_i^r - \boldsymbol{\mu}_r)^\top \quad (34)$$

$$\mu_s = \frac{1}{m} \sum_{j=1}^m \mathbf{z}_j^s, \quad \Sigma_s = \frac{1}{m-1} \sum_{j=1}^m (\mathbf{z}_j^s - \mu_s)(\mathbf{z}_j^s - \mu_s)^\top \quad (35)$$

The Fréchet Distance between these distributions is then computed as:

$$\text{FD} = \|\mu_r - \mu_s\|_2^2 + \text{Tr}(\Sigma_r + \Sigma_s - 2(\Sigma_r \Sigma_s)^{1/2}) \quad (36)$$

where  $\text{Tr}(\cdot)$  denotes the matrix trace and  $(\Sigma_r \Sigma_s)^{1/2}$  is the matrix square root of  $\Sigma_r \Sigma_s$ .

### J.3.3 Interpretation

This metric captures both the difference in means (first term) and the difference in covariance structure (second term) between real and synthetic gene expression profiles in the reduced PCA space. Lower values indicate better agreement between the distributions, suggesting higher quality synthetic data. The use of PCA ensures that the comparison focuses on the most significant sources of variation in the gene expression data while reducing computational complexity from  $O(d^2)$  to  $O(k^2)$  where typically  $k \ll d$ .

## J.4 Pearson Correlation Coefficient (PCC)

While MMD and Wasserstein distances measure distributional differences, the Pearson correlation coefficient quantifies linear relationships between paired observations. For two random variables  $X$  and  $Y$ , the population Pearson correlation coefficient is defined as:

$$\rho_{X,Y} = \frac{\text{Cov}(X, Y)}{\sigma_X \sigma_Y} = \frac{\mathbb{E}[(X - \mu_X)(Y - \mu_Y)]}{\sqrt{\mathbb{E}[(X - \mu_X)^2]} \sqrt{\mathbb{E}[(Y - \mu_Y)^2]}}, \quad (37)$$

where  $\mu_X, \mu_Y$  are the means and  $\sigma_X, \sigma_Y$  are the standard deviations. Given paired samples  $\{(x_i, y_i)\}_{i=1}^n$ , the sample correlation coefficient is:

$$r = \frac{\sum_{i=1}^n (x_i - \bar{x})(y_i - \bar{y})}{\sqrt{\sum_{i=1}^n (x_i - \bar{x})^2} \sqrt{\sum_{i=1}^n (y_i - \bar{y})^2}}, \quad (38)$$

where  $\bar{x} = \frac{1}{n} \sum_{i=1}^n x_i$  and  $\bar{y} = \frac{1}{n} \sum_{i=1}^n y_i$ . The coefficient  $r \in [-1, 1]$ , with  $|r| = 1$  indicating perfect linear relationship and  $r = 0$  suggesting no linear correlation. For multivariate data  $\mathbf{X} \in \mathbb{R}^{n \times d}$  and  $\mathbf{Y} \in \mathbb{R}^{n \times d}$ , one can compute the average correlation across dimensions or construct a correlation matrix. While Pearson correlation captures only linear dependencies and is sensitive to outliers, it remains widely used due to its computational efficiency and interpretability in assessing feature-wise relationships between datasets.

## J.5 Metrics used in experiments

**Reconstruction Metrics** In our experiments, we use the reconstruction error for the Negative Binomial distribution, PCC and Mean Squared Errors (MSE) as reconstruction metrics.

**Generation Metrics** For evaluating generation capabilities of models, we use the MMD with the RBF kernel, the Wasserstein Distance, and the Fréchet Distance, all calculated to 30 principal components. We compute the PCA on the true data, and project generated data using the loadings. All evaluations were run using 3 generation seeds.

**Perturbation Metrics** For evaluating perturbation prediction capabilities of models, we used the overlap of DEG (Differentially Expressed Genes) which is related to correlation of average treatment effect ATE-Pearson  $r$  in [6], the Spearman Correlation of Log2Fold Changes of significant DEGs, the discrimination L1 score and the Mean Absolute Error (MAE), all computed using the `cell-eval` [5] library. All evaluations were run using 3 model outputs, generated for 3 different seeds. For scLDM, we simply sampled from the same model 3 times using different seeds. For all other models, we retrained the model from scratch with different seeds, which only impacts initialization, since the dataset split is fixed.

## K Ablation on type of Classifier-Free Guidance

**Classifier-Free Guidance with Multiple Conditioning Variables.** In our setting, as described in section 4.2 the diffusion model is conditioned on multiple attributes simultaneously (e.g., cell type and perturbation). We explore two alternative strategies for applying classifier-free guidance (CFG):

**(Type I: Joint conditioning).** A single conditioning token is assigned to each unique combination of attributes. The model output under this strategy is given by

$$\tilde{v}_{t,\epsilon}(\mathbf{Z}, y) = v_{t,\epsilon}(\mathbf{Z}; \text{Null}) + \omega [v_{t,\epsilon}(\mathbf{Z}; y) - v_{t,\epsilon}(\mathbf{Z}; \text{Null})], \quad (39)$$

where  $y$  encodes the full joint condition (e.g., “CD4 Naive + IL-9” or “HepG2 + PPP6C”).

**(Type II: Additive conditioning).** Instead of encoding combinations directly, we treat each conditioning variable independently. For  $M$  attributes with labels  $\{y^{(j)}\}_{j=1}^M$ , the guided output is

$$\tilde{v}_{t,\epsilon}(\mathbf{Z}, \{y^{(j)}\}_{j=1}^M) = v_{t,\epsilon}(\mathbf{Z}; \text{Null}) + \sum_{j=1}^M \omega_j [v_{t,\epsilon}(\mathbf{Z}; y^{(j)}) - v_{t,\epsilon}(\mathbf{Z}; \text{Null})], \quad (40)$$

where each attribute contributes an additive adjustment relative to the unconditional prediction.

**Empirical Comparison.** We evaluate both approaches on **Parse 1M** (conditioning on cell type + cytokine perturbation) and **Replogle** (conditioning on cell type + gene knockout). As shown in Table 15, the joint conditioning strategy (Type I) consistently outperforms the additive conditioning strategy (Type II) across metrics, indicating that learning a single joint embedding for each combination of attributes is more effective in capturing complex context-perturbation interactions than treating them independently.

In all experiments, we set the guidance weight  $\omega$  to 1, unless specified otherwise, and we did not tune this parameter.

## L Additional Results

### L.1 Experiment 1: Ablation experiments and additional results

In Table 12 we report an ablation study on encoding gene expression following our approach of zero padding the non-expressed genes (see Appendix F.1), or utilizing the full context as input, as typically done in scVI. Our approach is superior in terms of reconstruction performance, as well as more computationally efficient.

TABLE 12. Reconstruction performance comparison of our scLDM using the zero padding strategy for encoding, or using all genes as input.

Dataset	Model	RE ↓	PCC ↑	MSE ↓
Dentate Gyrus	full context	5458.6	0.097	0.252
	zero padding	<b>5325.3</b>	<b>0.125</b>	<b>0.242</b>

In Figure 4, we report another ablation study on hyperparameters of the VAE architecture: we sweep over depth (number of layers for the encoder/decoder layers), width (embedding dimensions) and number

of latent tokens, over two datasets that consists of vastly different number of genes (18k for dentate gyrus versus 2k for replogle) and cells (600k for replogle and 18k for dentate gyrus). Interestingly, depth appears to negatively impact performance in the dentate gyrus dataset, whereas it does not in the Replogle dataset. For both datasets, a larger embedding dimension as well as a higher number of latent tokens improve performance.

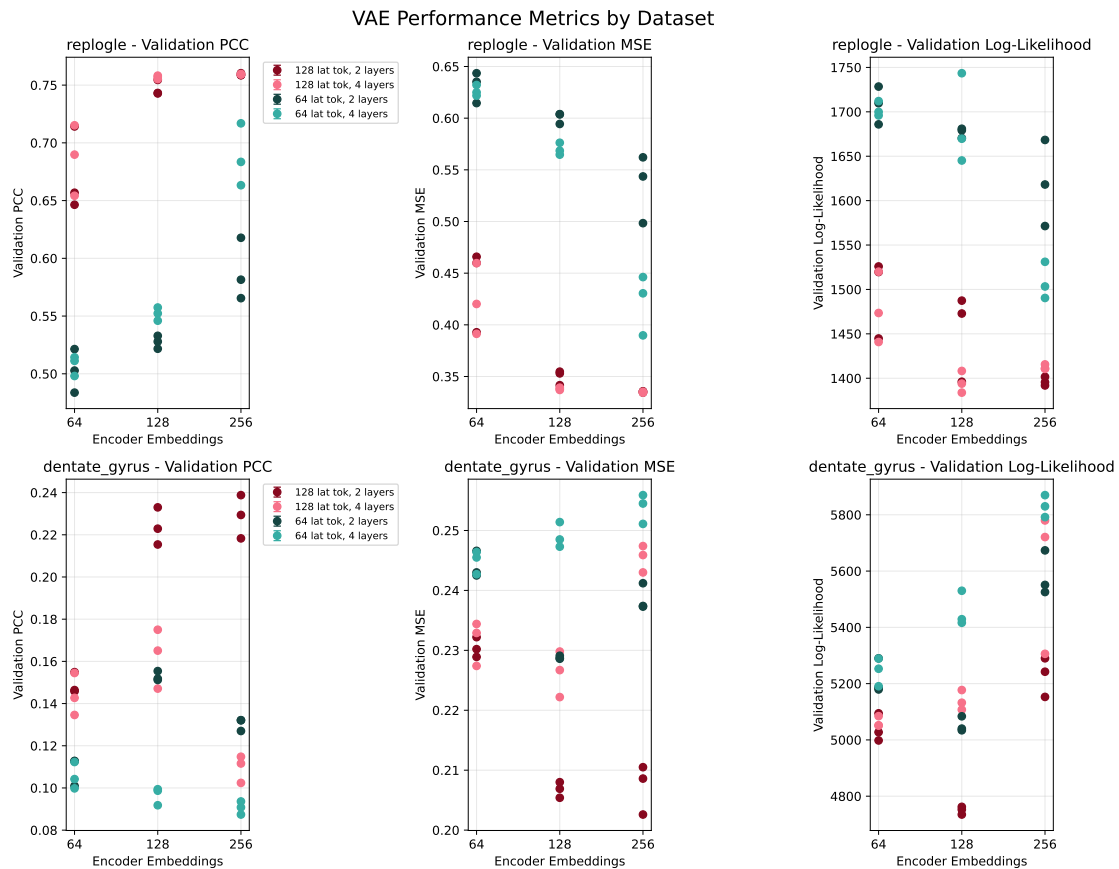


FIGURE 4. Ablations on VAE width, depth and number of latent tokens

In Table 13, we present the model comparison on benchmark datasets, but on all genes. Please note that in this comparison, scDiffusion performs better than in the table on the metrics computed only on highly variable genes. The reason for that is that the data is extremely sparse, and the model synthesizes data consisting mostly of zeros. As a result, the match becomes better. This is a clear indication of deficiencies of the currently used evaluation metrics for generative models, which is a long-standing issue in the field [67].

In Figure 5, 6, and 7, we present a visualization of gene-wise variance for true and generated data on Dentate Gyrus, Tabula Muris, and HLCA, respectively. CFGen and scLDM properly recover true variance, with a slight tendency of scLDM to overestimate, while scDiffusion completely fails and underestimates the true Variance.

In Figure 8, we present a visualization of true and generated data for all models and all datasets in UMAP coordinates. In Figures 9 10 11, we present the conditional generation results in UMAP coordinates colored by the conditional class.

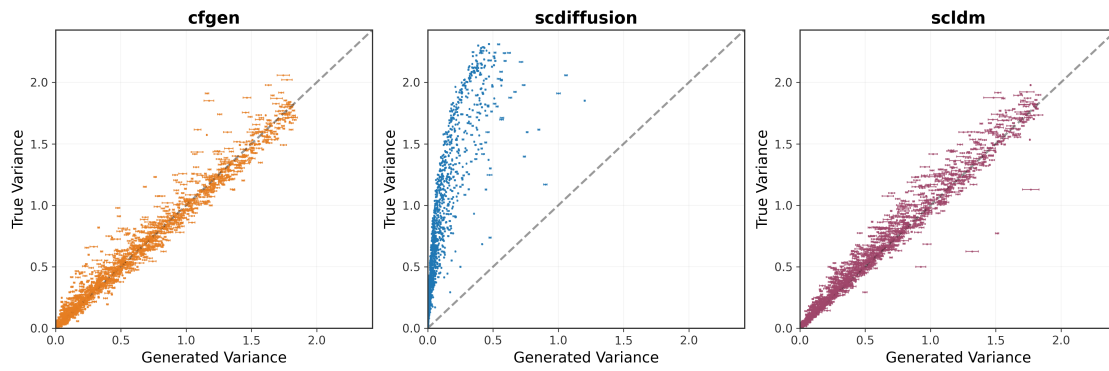


FIGURE 5. Visualization of the gene-wise variance for true and generated data for CFGen (left), scDiffusion (middle) our model (right), for the conditional generation settings on Dentate Gyrus. The error bars represent the standard errors over 3 seeds.

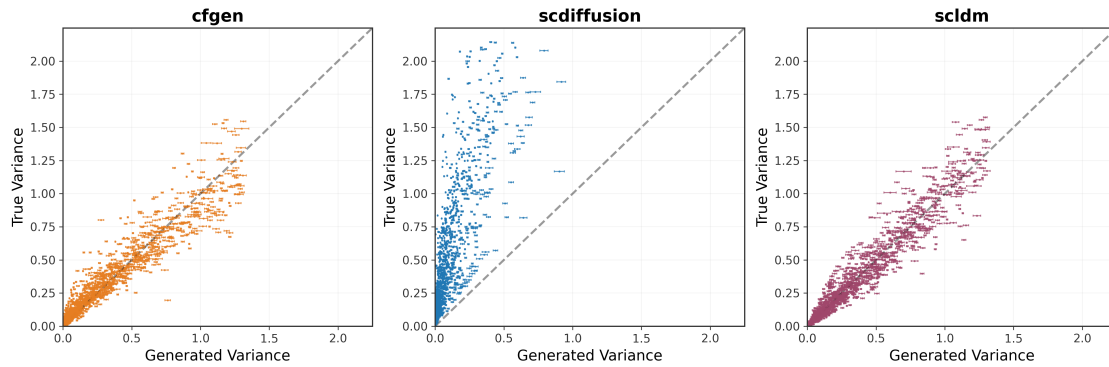


FIGURE 6. Visualization of the gene-wise variance for true and generated data for CFGen (left), scDiffusion (middle) our model (right), for the conditional generation settings on Tabula Muris. The error bars represent the standard errors over 3 seeds.

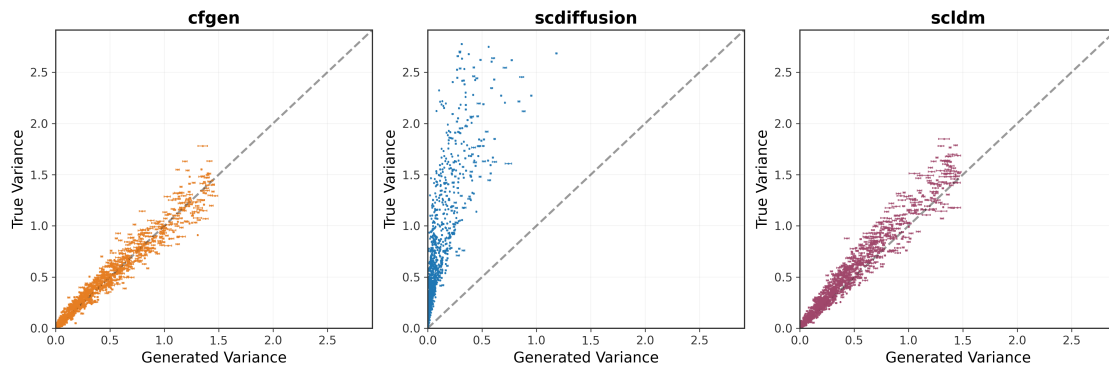


FIGURE 7. Visualization of the gene-wise variance for true and generated data for CFGen (left), scDiffusion (middle) our model (right), for the conditional generation settings on HLCA. The error bars represent the standard errors over 3 seeds.

TABLE 13. Model performance comparison on unconditional and conditional cell generation benchmarks on all genes. W2, MMD<sup>2</sup> RBF and FD metrics calculated on 30 principal components are reported (lower is better).

Setting	Model	W2 ↓	MMD <sup>2</sup> RBF ↓	FD ↓
Dentate Gyrus				
Uncond	scDiffusion	8.545 ± 0.061	0.021 ± 0.000	16.303 ± 0.265
	CFGen	11.396 ± 0.025	0.027 ± 0.001	24.942 ± 0.456
	Ours	9.489 ± 0.054	0.027 ± 0.000	28.307 ± 0.357
Cond	scDiffusion	8.906 ± 0.041	0.093 ± 0.001	28.829 ± 1.612
	CFGen	10.580 ± 0.022	0.082 ± 0.001	40.298 ± 0.472
	Ours	9.147 ± 0.024	0.108 ± 0.004	31.045 ± 0.884
Tabula Muris				
Uncond	scDiffusion	8.616 ± 0.215	0.002 ± 0.000	6.881 ± 0.565
	CFGen	11.331 ± 0.081	0.009 ± 0.000	31.788 ± 1.073
	Ours	10.573 ± 0.092	0.005 ± 0.000	17.641 ± 0.337
Cond	scDiffusion	11.459 ± 0.081	0.035 ± 0.001	43.456 ± 1.678
	CFGen	9.420 ± 0.041	0.026 ± 0.001	22.045 ± 0.389
	Ours	8.530 ± 0.110	0.019 ± 0.001	15.547 ± 0.557
HLCA				
Uncond	scDiffusion	9.234 ± 0.008	0.002 ± 0.000	5.585 ± 0.180
	CFGen	12.651 ± 0.025	0.008 ± 0.000	24.038 ± 0.492
	Ours	10.816 ± 0.089	0.010 ± 0.000	24.126 ± 0.473
Cond	scDiffusion	9.998 ± 0.048	0.094 ± 0.002	40.093 ± 3.103
	CFGen	10.715 ± 0.039	0.087 ± 0.005	36.178 ± 0.961
	Ours	9.350 ± 0.046	0.084 ± 0.005	28.398 ± 1.358

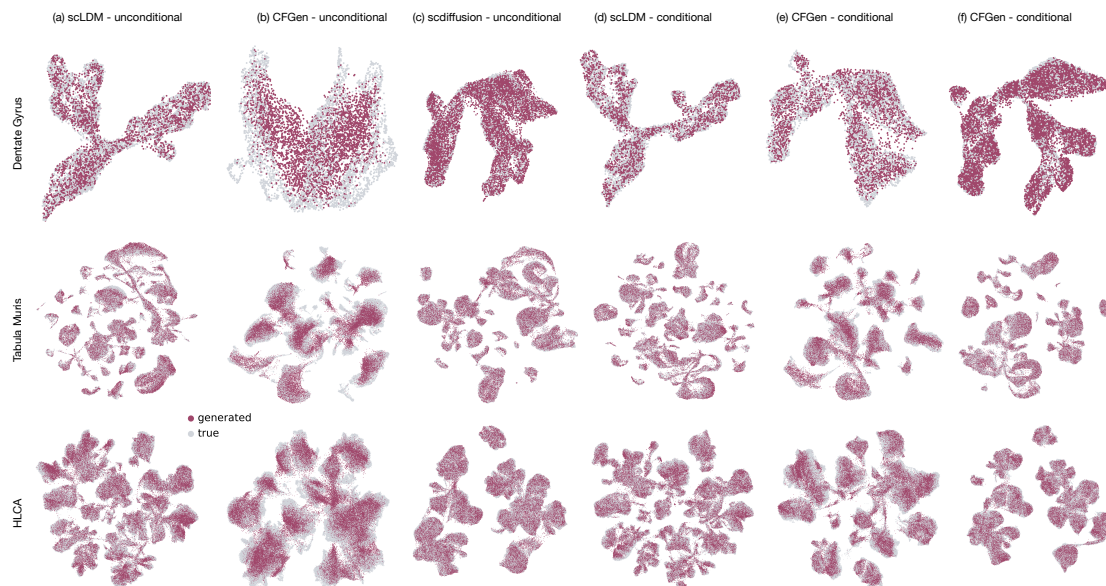


FIGURE 8. Visualization of the generation results for all datasets and models for conditional and unconditional generations. True and Generated gene expression is embedded in UMAP coordinates jointly, upon normalization, following standard Scanpy pipeline.

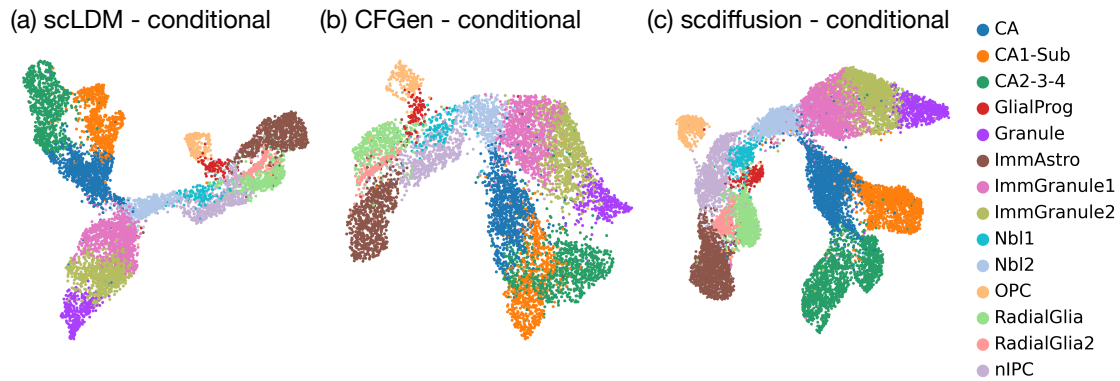


FIGURE 9. Visualization of the conditional generation results for the dentate gyrus dataset and all models, colored by the conditional label (clusters).

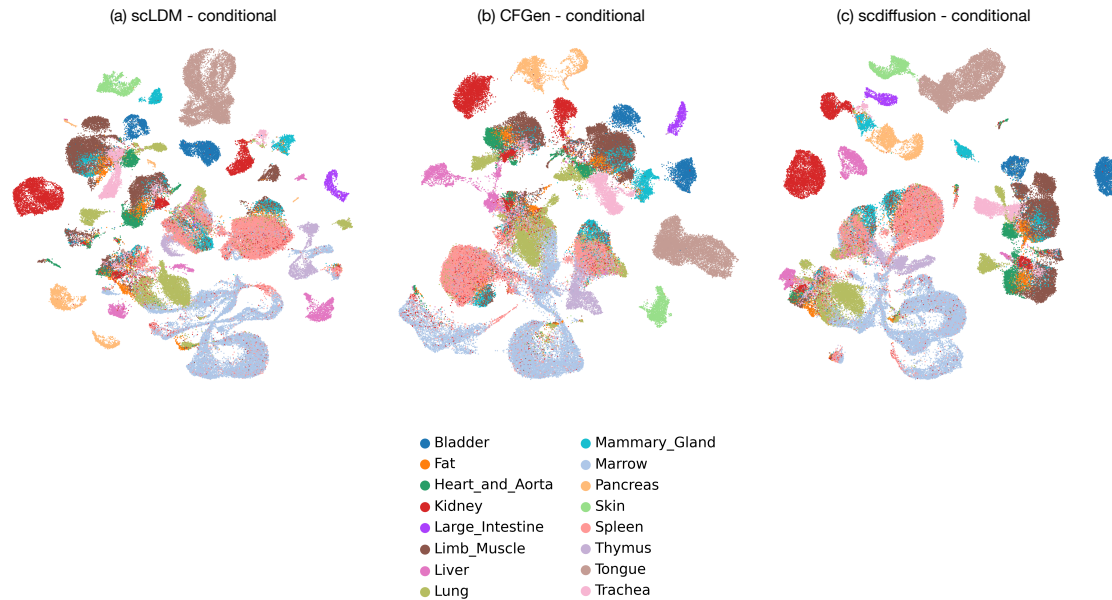


FIGURE 10. Visualization of the conditional generation results for the tabula muris dataset and all models, colored by the conditional label (tissue).

## L.2 Experiment 1: Interpretability results on cross-attention scores

The cross-attention encoder and decoder layers can be interpreted as pooling and unpooling operators on the gene tokens at input and output. The attention scores of the cross attention layers provide an interpretability tool to analyze how gene tokens map to the latent tokens. We analyzed the attention patterns of the encoder and decoder cross-attention layers in the dentate gyrus dataset. To this end, we computed the marker genes for each cell type annotated in the dataset. We further extracted the attention weights between the gene tokens and the latent tokens and averaged them across 1k cells (where each celltype was sampled roughly the same proportion with respect to the original dataset). Using the genes v. latent tokens average attention matrix, we computed enrichment scores for the cell type markers for each latent token using decoupler [68]. We visualized the enrichment score between each latent token and cell-type marker genes in Figure 12, where each column (latent tokens) and rows (marker genes gene set) was clustered using hierarchical clustering. We can observe that the latent tokens do show a selective enrichment for marker genes of specific

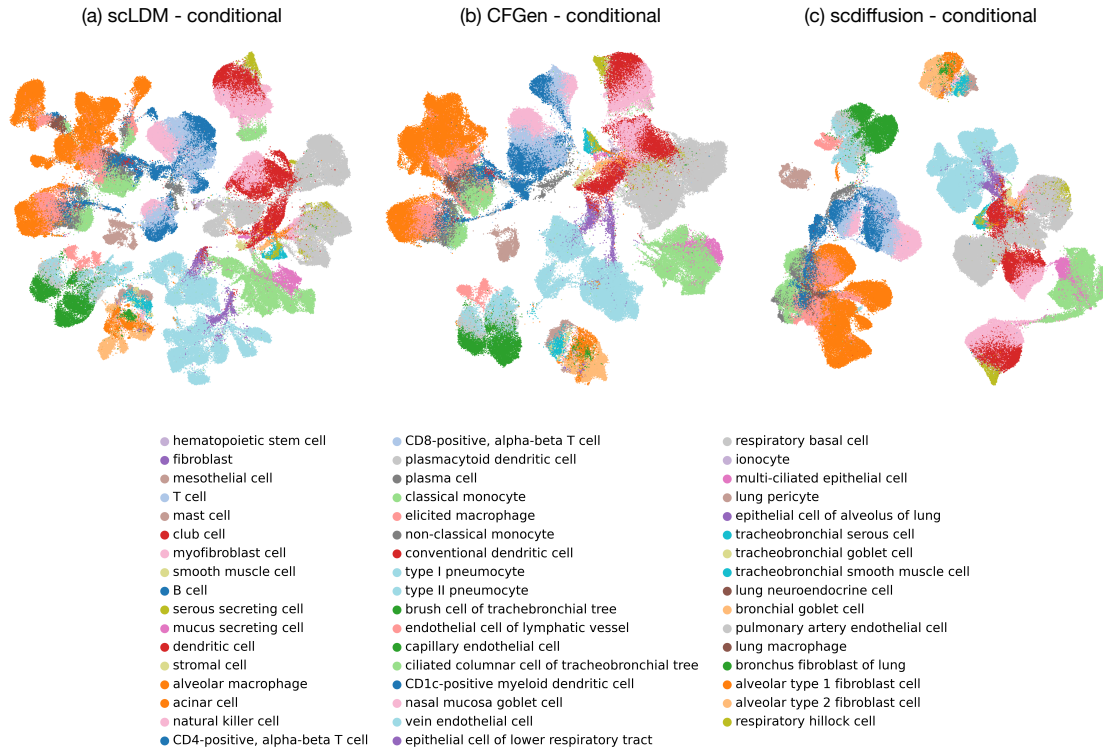


FIGURE 11. Visualization of the conditional generation results for the hlca dataset and all models, colored by the conditional label (cell type).

cell types. In particular, the enrichment score seems to separate correctly the groups of cell types belonging to the Neuron, Oligodendrocyte and Glia lineage, both in the encoder and decoder layer.

### L.3 Experiment 2: Reconstruction capabilities on perturbation datasets

The results presented in Table 14 demonstrate that our proposed approach significantly outperforms the scVI baseline across all evaluated metrics on the Parse1M and Replogle dataset. Most notably, our method achieves a substantially lower reconstruction error (RE) of about 310 nats compared to scVI’s 432 nats, indicating better reconstructive capabilities. Furthermore, our approach yields a remarkable improvement in Pearson correlation coefficient (PCC), achieving 0.887 versus scVI’s mediocre 0.351, which suggests that our model captures the underlying biological relationships much more effectively. The mean squared error (MSE) is also greatly reduced from 0.701 to 0.188, representing an approximately 73% reduction in reconstruction error. These consistent improvements across multiple evaluation criteria provide strong evidence that our method offers substantial advantages over scVI and indicate its great potential in analyzing biological data.

TABLE 14. Model performance comparison on cell reconstruction task.

Dataset	Model	RE ↓	PCC ↑	MSE ↓
Parse 1M	scVI	432.41 ± 0.08	0.351 ± 0.000	0.701 ± 0.001
	scLDM	<b>149.70 ± 0.22</b>	<b>0.874 ± 0.003</b>	<b>0.165 ± 0.002</b>
Replogle	scVI	2144.86 ± 0.35	0.166 ± 0.000	0.703 ± 0.001
	scLDM	<b>1590.51 ± 0.38</b>	<b>0.713 ± 0.004</b>	<b>0.285 ± 0.002</b>



FIGURE 12. Enrichment scores for marker genes of cell-types in the dataset of cross-attention for both the cross-attention encoder and decoder layers.

#### L.4 Experiment 2: A comparison between *additive* and *joint* conditioning in classifier-free guidance

Table 15 compares the performance of our scLDM model using two different classifier-free guidance approaches for conditional cell generation: the additive steering method proposed by Palma et al. [20] and our joint attribute steering method. Across all metrics (Wasserstein-2 distance,  $MMD^2$  RBF, and Fréchet Distance) and both datasets (Parse 1M and Replogle), the joint approach consistently outperforms the additive approach, demonstrating substantial improvements in generation quality.

TABLE 15. Model performance comparison on conditional cell generation on Parse1M and Replogle. For these results scLDM was trained using the classifier-free guidance approach proposed in [20] (additive) and ours (joint).

Dataset	Model	W2 ↓	$MMD^2$ RBF ↓	FD ↓
Parse 1M	scLDM (additive)	15.850 ± 0.073	0.129 ± 0.004	109.196 ± 2.933
	scLDM (joint)	<b>12.455</b> ± 0.001	<b>0.027</b> ± 0.000	<b>18.145</b> ± 0.068
Replogle	scLDM (additive)	18.538 ± 0.058	0.451 ± 0.003	255.510 ± 2.163
	scLDM (joint)	<b>11.288</b> ± 0.011	<b>0.200</b> ± 0.001	<b>53.555</b> ± 0.210

#### L.5 Experiment 2: Perturbation prediction metrics

We further evaluated our models and all baselines on the generated results for the test set perturbations using the `cell-eval` package <sup>7</sup> (Figure 13). Our model, although not explicitly designed for perturbation prediction, is competitive across various metrics compared to the baselines on both datasets considered.

<sup>7</sup><https://github.com/ArcInstitute/cell-eval>

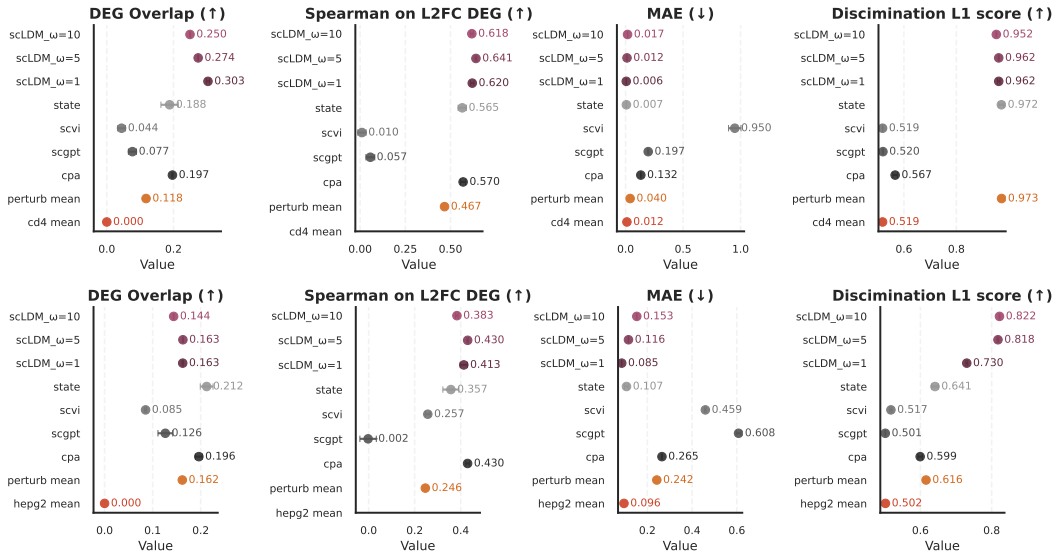


FIGURE 13. Evaluation metrics from the `cell-eval` package for the Parse 1M dataset (top) and Replogle dataset (bottom)

## L.6 Experiment 3

For the last experiment, we trained three VAEs for our approach (scLDM-VAE): with 20M parameters, 70M parameters, and 270M parameters. Further, we evaluated the resulting models using embeddings on a downstream task (classification) for two out-of-distribution datasets (COVID-19 and Tabula Sapiens 2.0).

First, we evaluated these three versions of our model using reconstruction metrics on the dataset they were trained on, namely, Human Census Data from CellxGene<sup>8</sup>. Looking at Table 16, we can see a clear relationship between model size and reconstruction performance for the scLDM-VAE models on the CellxGene dataset. As the number of parameters increases from 20M to 270M, all three metrics show substantial improvement: reconstruction error (RE) decreases, Pearson correlation coefficient (PCC) increases, and mean squared error (MSE) drops. These results demonstrate that scaling up the scLDM-VAE architecture yields consistent performance gains across all reconstruction metrics, with the 270M parameter model achieving approximately 17% lower reconstruction error and 18% higher correlation compared to the smallest 20M model.

TABLE 16. Reconstruction performance comparison of our scLDM-VAEs with varying number of parameters: 20M, 70M, and 270M.

Dataset	Model	RE ↓	PCC ↑	MSE ↓
CellxGene Census	scLDM-VAE (20M)	1742.7	0.661	0.137
	scLDM-VAE (70M)	1552.7	0.739	0.106
	scLDM-VAE (270M)	<b>1441.7</b>	<b>0.783</b>	<b>0.091</b>

Table 17 presents a comprehensive performance comparison of various models on the COVID-19 dataset, averaged across all donors. Our scLDM model with 270M parameters achieves the best performance across all metrics (ROC AUC, PR AUC, F1 Score, Recall, and Precision), demonstrating consistent improvements over both transformer-based baselines (TranscriptFormer, scGPT, Geneformer, UCE) and traditional VAE approaches (scVI, AIDO.Cell).

Figure 14 visualizes the receiver operating characteristic (ROC) and precision-recall (PR) curves for all models on the COVID-19 classification task. The curves further illustrate the superior discriminative

<sup>8</sup><https://cellxgene.cziscience.com/>

TABLE 17. COVID-19 Model Performance Summary (Averaged Across All Donors). **Bold** indicates the best performing model.

Model	ROC AUC	PR AUC	F1 Score	Recall	Precision
scLDM (270M)	<b>0.909</b> $\pm$ 6e-04	<b>0.877</b> $\pm$ 0.001	<b>0.820</b> $\pm$ 0.001	<b>0.836</b> $\pm$ 0.001	<b>0.806</b> $\pm$ 0.001
TranscriptFormer	0.905 $\pm$ 4e-04	0.874 $\pm$ 9e-04	0.814 $\pm$ 0.002	0.829 $\pm$ 0.003	0.801 $\pm$ 0.001
scLDM (70M)	0.905 $\pm$ 5e-04	0.872 $\pm$ 0.001	0.815 $\pm$ 0.001	0.83 $\pm$ 0.002	0.801 $\pm$ 0.001
scLDM (20M)	0.902 $\pm$ 5e-04	0.869 $\pm$ 0.001	0.811 $\pm$ 0.001	0.827 $\pm$ 0.001	0.797 $\pm$ 0.002
UCE	0.876 $\pm$ 5e-04	0.834 $\pm$ 0.002	0.775 $\pm$ 8e-04	0.781 $\pm$ 0.001	0.771 $\pm$ 0.002
scGPT	0.876 $\pm$ 4e-04	0.831 $\pm$ 0.001	0.779 $\pm$ 9e-04	0.793 $\pm$ 0.002	0.766 $\pm$ 0.001
Geneformer	0.866 $\pm$ 6e-04	0.815 $\pm$ 0.001	0.768 $\pm$ 0.001	0.781 $\pm$ 0.003	0.757 $\pm$ 0.001
AIDO.Cell	0.821 $\pm$ 7e-04	0.753 $\pm$ 9e-04	0.717 $\pm$ 8e-04	0.729 $\pm$ 0.002	0.708 $\pm$ 0.001
scVI	0.800 $\pm$ 7e-04	0.709 $\pm$ 0.001	0.675 $\pm$ 0.001	0.680 $\pm$ 0.002	0.680 $\pm$ 0.001

performance of scLDM variants, with the 270M parameter model achieving the highest area under both curves, consistent with the quantitative results in Table 17.

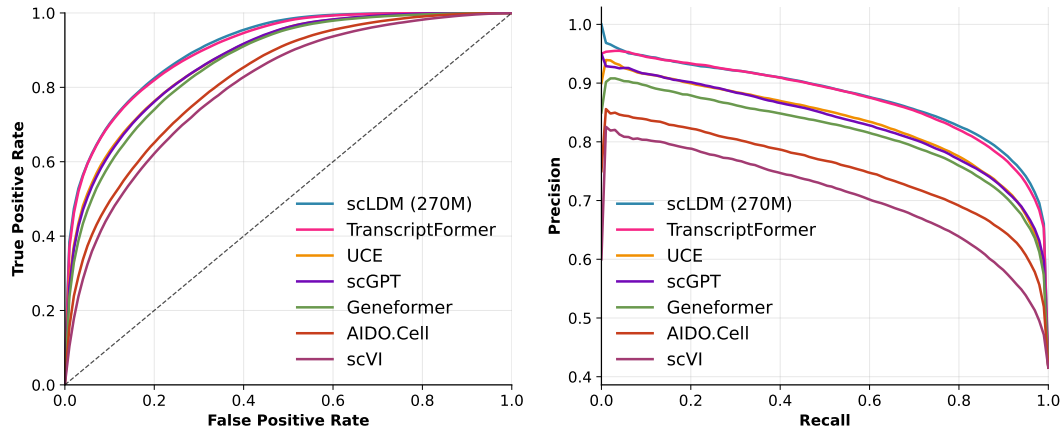


FIGURE 14. Precision-recall and receiver operator curves for COVID-19 data.

Table 18 summarizes model performance on the Tabula Sapiens 2.0 dataset, averaged across all tissues. Notably, the smallest scLDM variant (20M parameters) achieves the highest F1 score (0.804), slightly outperforming both larger scLDM models and all baseline methods, suggesting that model scale may have diminishing returns on this particular cell type classification task.

TABLE 18. Tabula Sapiens 2.0 model performance summary (averaged across all tissues)

Model	F1 Score	Recall	Precision
scLDM-20M	<b>0.804</b> $\pm$ 0.002	<b>0.805</b> $\pm$ 0.002	<b>0.812</b> $\pm$ 0.002
scLDM-270M	0.802 $\pm$ 0.002	0.803 $\pm$ 0.002	0.811 $\pm$ 0.002
scLDM-70M	0.802 $\pm$ 0.002	0.802 $\pm$ 0.002	0.810 $\pm$ 0.002
scGPT	0.800 $\pm$ 0.002	0.802 $\pm$ 0.002	0.806 $\pm$ 0.002
scVI	0.799 $\pm$ 0.002	0.794 $\pm$ 0.002	0.814 $\pm$ 0.003
TranscriptFormer	0.799 $\pm$ 0.002	0.800 $\pm$ 0.002	0.802 $\pm$ 0.002
UCE	0.796 $\pm$ 0.002	0.797 $\pm$ 0.001	0.801 $\pm$ 0.003
Geneformer	0.777 $\pm$ 0.002	0.776 $\pm$ 0.002	0.786 $\pm$ 0.003
AIDO.Cell	0.724 $\pm$ 0.002	0.715 $\pm$ 0.002	0.748 $\pm$ 0.003